J|A|C|S
A R T I C L E S

Two-Dimensional Networks Based on Mn_4 Complex Linked by Dicyanamide Anion: From Single-Molecule Magnet to Classical Magnet Behavior

Hitoshi Miyasaka,*[,†,‡] Kazuya Nakata,[†] Lollita Lecren,[||] Claude Coulon,[||]
Yasuhiro Nakazawa,[§] Tatsuya Fujisaki,[§] Ken-ichi Sugiura,[†]
Masahiro Yamashita,[⊥] and Rodolphe Clérac*[,||]

Contribution from the Department of Chemistry, Graduate School of Science, Tokyo Metropolitan University, 1-1 Minamiohsawa, Hachioji, Tokyo 192-0397, Japan, PRESTO and CREST, the Japan Science and Technology Agency (JST), 4-1-8 Honcho, Kawaguchi, Saitama 332-0012, Japan, Centre de Recherche Paul Pascal, CNRS-UPR 8641, 115 Av. du Dr. A. Schweitzer, 33600 Pessac, France, Department of Chemistry, Graduate School of Science, Osaka University, 1-1 Machikaneyama, Toyonaka, Osaka 560-0043, Japan, and Department of Chemistry, Graduate School of Science, Tohoku University, Aramaki-Aza-Aoba, Aoba-ku, Sendai 980-8578, Japan

Received November 8, 2005; E-mail: miyasaka@comp.metro-u.ac.jp; clerac@crpp-bordeaux.cnrs.fr

---

Abstract: Three two-dimensional (2D) network compounds based on Mn^{III}/Mn^{II} tetranuclear single-molecule magnets (SMMs) connected by dicyanamide (dcn^-) linkers have been synthesized: $[Mn_4(hmp)_4(Hpdm)_2(dcn)_2](ClO_4)_2{\cdot}2H_2O{\cdot}2MeCN$ (**2**), $[Mn_4(hmp)_4Br_2(OMe)_2(dcn)_2]{\cdot}0.5H_2O{\cdot}2THF$ (**3**), $[Mn_4(hmp)_6(dcn)_2](ClO_4)_2$ (**4**), where Hhmp and H_2pdm are 2-hydroxymethylpyridine and pyridine-2,6-dimethanol, respectively. The $[Mn_4]/dcn^-$ system appears very versatile, but enables its chemistry to be rationalized by a fine-tune of the synthetic conditions. The double cuboidal $[Mn_4]$ unit is preserved in the whole family of compounds, despite strong modifications of its Mn^{II} coordination sphere. The chemical control of the coordination number of dcn^- on the Mn^{II} sites has been the key to obtain the following series of compounds: a discrete cluster, $[Mn_4(hmp)_6(NO_3)_2(dcn)_2]{\cdot}2MeCN$ (**1**), 2D networks (**2**, **3**, and **4**), and the previously reported 3D compound, $[Mn_4(hmp)_4(\mu_3\text{-}OH)_2][Mn^{II}(dcn)_6]{\cdot}2MeCN{\cdot}THF$. Direct current magnetic measurements show that both Mn^{2+}—Mn^{3+} and Mn^{3+}—Mn^{3+} intra-$[Mn_4]$ magnetic interactions are ferromagnetic leading to an $S_T = 9$ ground state for the $[Mn_4]$ unit. Despite the very similar 2D lattices in **2**−**4**, the two kinds of orientation of the $[Mn_4]$ unit (i.e., angle variations between the two easy axes) lead to different magnetic properties ranging from SMM behavior for **2** and **1** to a long-range canted antiferromagnetic order for **4**. Compound **3** is more complicated as the magnetic measurements strongly suggest the presence of a canted antiferromagnetic order below 2.1 K, although the magnetization slow relaxation is simultaneously observed. Heat capacity measurements confirm the long-range magnetic order in **4**, while in **3**, the critical behavior is frozen by the slow relaxation of the anisotropic $[Mn_4]$ units.

Introduction

Since the beginning of the 1990s, high-spin complexes exhibiting "Single-Molecule Magnet" (SMM) behavior have received a wide attention not only for their interests in fundamental physics, but also for their potential application in information storage or devices for future quantum computers.[1−3] Actually, extensive investigations of these SMMs have revealed their unique magnetic properties such as magnetization slow relaxation with thermal and quantum regimes,[1−2] quantum tunneling of the magnetization (QTM),[4] and quantum phase interferences.[5] In comparison to classical superparamagnetic

---

[†] Tokyo Metropolitan University.

[‡] PRESTO and CREST, JST.

[||] Centre de Recherche Paul Pascal.

[§] Osaka University and CREST, JST.

[⊥] Tohoku University and CREST, JST.

(1) (a) Boyd, P. D. W.; Li, Q.; Vincent, J. B.; Folting, K.; Chang, H.-R.; Streib, W. E.; Huffman, J. C.; Christou, G.; Hendrickson, D. N. *J. Am. Chem. Soc.* **1988**, *110*, 8537. (b) Caneschi, A.; Gatteschi, D.; Sessoli, R. *J. Am. Chem. Soc.* **1991**, *113*, 5873. (c) Sessoli, R.; Tsai, H.-L.; Schake, A. R.; Wang, S.; Vincent, J. B.; Folting, K.; Gatteschi, D.; Christou, G.; Hendrickson, D. N. *J. Am. Chem. Soc.*, **1993**, *115*, 1804.

(2) (a) Christou, G.; Gatteschi, D.; Hendrickson, D. N.; Sessoli, R. *MRS Bull.* **2000**, 66. (b) Gatteschi, D.; Sessoli, R. *Angew. Chem., Int. Ed.* **2003**, *42*, 268.

(3) Leuenberger, M. N.; Loss, D. *Nature* **2001**, *410*, 789.

(4) (a) Friedman, J. R.; Sarachik, M. P.; Tejada, J.; Maciejewski, J.; Ziolo, R. *J. Appl. Phys.* **1996**, *79*, 6031. (b) Thomas, L.; Lionti, F.; Ballou, R.; Gatteschi, D.; Sessoli, R.; Barbara, B. *Nature* **1996**, *383*, 145. (c) Friedman, J. R.; Sarachik, M. P.; Tejada, J.; Ziolo, R. *Phys. Rev. Lett.* **1996**, *76*, 3830. (d) Hernández, J. M.; Zhang, X. X.; Luis, F.; Bartolomé, J.; Tejada, J.; Ziolo, R. *Europhys. Lett.* **1996**, *35*, 301. (e) Friedman, J. R.; Sarachik, M. P.; Hernandez, J. M.; Zhang, X. X.; Tejada, J.; Molins, E.; Ziolo, R. *J. Appl. Phys.* **1997**, *81*, 3978.

(5) (a) Wernsdorfer, W.; Sessoli, R. *Science* **1999**, *284*, 133. (b) Wernsdorfer, W.; Sessoli, R.; Caneschi, A.; Gatteschi, D.; Cornia, A.; Mailly, D. *J. Appl. Phys.* **2000**, *87*, 5481. (c) Wernsdorfer, W.; Soler, M.; Christou, G.; Hendrickson, D. N. *J. Appl. Phys.* **2002**, *91*, 7164. (d) Lecren, L.; Wernsdorfer, W.; Li, Y.-G.; Roubeau, O.; Miyasaka, H.; Clérac, R. *J. Am. Chem. Soc.* **2005**, *127*, 11311. (e) Wernsdorfer, W.; Chakov, N. E.; Christou, G. *Phys. Rev. Lett.* **2005**, *95*, 037203.

10.1021/ja0574062 CCC: $33.50

nanoparticles, SMMs can be chemically tailored at the molecular level (using ligand- or metal-substitution, redox activity on metal centers, etc.), and thereby, well-defined physical properties (i.e., quantum properties) can be obtained. On the other hand, it seems also extremely interesting to control interactions between SMM molecules and thus to design new magnetic nano-objects or networks using already known SMMs as building blocks. Recently, Wernsdorfer and others have reported on a dimer of antiferromagnetically coupled SMMs. They showed that the magnetic interactions were able to tune the quantum properties of the original SMM unit.[6] This exciting conclusion was also made in an extended network of SMMs that was magnetically connected by weak interactions (such as hydrogen bonds) mediating antiferromagnetic or ferromagnetic exchange.[7] These breakthroughs open new perspectives to introduce magnetic interactions between SMM molecules in desired architectures. The control of the network dimensionality on such SMM architectures may also provide a unique opportunity to investigate new magnetic behaviors and also the frontier between SMMs and classical bulk magnets.

In this line, we have been working in the past few years on introducing covalent bonds between SMM units to control the magnitude of the inter-SMM magnetic interaction. Among the known SMMs favorable for this approach, we have chosen $Mn^{II}_2Mn^{III}_2$ mixed-valence tetranuclear SMMs reported first by Hendrickson and Christou in 2001: $[Mn_4(hmp)_6Br_2(H_2O)_2]Br_2\cdot 4H_2O$ (hmp$^-$ stands for the anion of 2-hydroxymethylpyridine, Hhmp).[8a,b] This type of compound[5d,8c,9] possesses a similar double-cuboidal $[Mn_4]$ core with various terminal ligands that are always either coordinating anions and/or solvent molecules on its Mn^{II} sites. Using these labile Mn^{II} sites, we have carried out syntheses and studies of more specimens of this family with the goal of linking them in a controlled manner. In 2004, we have successfully synthesized the first covalently linked SMM-based magnet: $[Mn_4(hmp)_4(\mu_3\text{-}OH)_2][Mn^{II}(dcn)_6]\cdot 2MeCN\cdot THF$ (where dcn$^-$ stands for the dicyanamide anion). This material that exhibits a long-range ferrimagnetic order at 4.1 K has a three-dimensional (3D) network based on two building-blocks, a $[Mn_4(hmp)_4(\mu_3\text{-}OH)_2]^{4+}$ SMM-type complex and a $[Mn^{II}\{N(CN)_2\}_6]^{4-}$ linking unit.[10] In 2005, Hendrickson et al. have synthesized a one-dimensional (1D) arrangement of $[Mn_4(hmp)_6]^{4+}$ SMMs bridged by chloride ions, which exhibited slow relaxation of the magnetization together with metamagnetic-like behavior.[11] These two recent examples illustrated nicely how the terminal ligands on the $[Mn_4]$ core are indeed easily exchangeable by appropriate bridging ligands that allow a controlled synthesis of materials with possible versatile networks and attractive magnetic properties.

Scheme 1. (a) Hhmp (2-Hydroxymethylpyridine) and H_2pdm (Pyridine-2,6-dimethanol); (b) $[Mn_4]$ Double Cuboidal Units Observed in **1**−**4**; L^1 and L^2 Are hmp$^-$ and NO_3^- in **1**; Hpdm$^-$ and dcn$^-$ in **2**; MeO$^-$ and Br$^-$/dcn$^-$ in **3**; hmp$^-$ and dcn$^-$ in **4**, Respectively

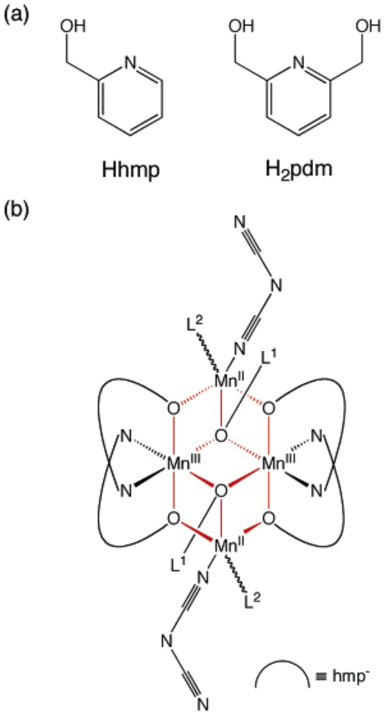

We herein report on the first three examples of two-dimensional (2D) network composed of the mixed-valence $[Mn_4]$ SMM-type complexes directly linked by the dicyanamide anions: $[Mn_4(hmp)_4(Hpdm)_2(dcn)_2](ClO_4)_2\cdot 2H_2O\cdot 2MeCN$ (**2**), $[Mn_4(hmp)_4Br_2(OMe)_2(dcn)_2]\cdot 0.5H_2O\cdot 2THF$ (**3**), and $[Mn_4(hmp)_6(dcn)_2](ClO_4)_2$ (**4**) (Hhmp and H_2pdm are shown in Scheme 1a). In parallel to these 2D materials, the discrete $[Mn_4(hmp)_6(dcn)_2(NO_3)_2]\cdot 2MeCN$ (**1**) complex possessing the terminal dicyanamide groups has also been obtained. The SMM behavior of this new discrete $[Mn_4]$ complex will be discussed in relation with the physical properties of the 2D compounds **2**−**4**.

Experimental Section

General Procedures and Materials. All chemicals and solvents were used as received; all preparations and manipulations were performed under aerobic conditions. Note for the synthesis of **3** that we used a new material $[Mn_4(hmp)_6Br_2(H_2O)_2]Br_2$ that will be described elsewhere. This compound was obtained reproductively using rigorously the method quoted in 8a. Despite our numerous attempts, we have been unable to obtain the solvated $[Mn_4(hmp)_6Br_2(H_2O)_2]Br_2\cdot 4H_2O$ complex.

Synthesis of $[Mn_4(hmp)_6(NO_3)_2(dcn)_2]\cdot 2MeCN$ (1). To an acetonitrile solution (20 mL) of manganese nitrate hexahydrate (287 mg, 1 mmol) was added 2-hydroxymethylpyridine (218 mg, 2 mmol) and 20 wt % water solution of tetraethylammonium hydroxide (736 mg, 1 mmol). After stirring for 1 h at room temperature, sodium dicyanamide (89 mg, 1 mmol) was added to the solution that was then further stirred for 1 h. The resulting solution was filtered, carefully layered on diglyme

---

(6) (a) Wernsdorfer, W.; Aliaga-Alcalde, N.; Hendrickson, D. N.; Christou, G. *Nature* **2002**, *416*, 406. (b) Wernsdorfer, W.; Bhaduri, S.; Tiron, R.; Hendrickson, D. N.; Christou, G. *Phys. Rev. Lett.* **2002**, *89*, 197201. (c) Park, K.; Pederson, M. R.; Richardson, S. L.; Aliaga-Alcalde, N.; Christou, G. *Phys. Rev. B* **2003**, *68*, 020405. (d) Hill, S.; Edwards, R. S.; Aliaga-Alcalde, N.; Christou, G. *Science* **2003**, *302*, 1015.

(7) (a) Tiron, R.; Wernsdorfer, W.; Aliaga-Alcalde, N.; Christou, G. *Phys. Rev. B* **2003**, *68*, 140407(R). (b) Tiron, R.; Wernsdorfer, W.; Foguet-Albiol, D.; Aliaga-Alcalde, N.; Christou, G. *Phys. Rev. Lett.* **2003**, *91*, 227203. (c) Boskovic, C.; Bircher, R.; Tregenna-Piggott, P. L. W.; Güdel, H. U.; Paulsen, C.; Wernsdorfer, W.; Barra, A.-L.; Khatsko, E.; Neels, A.; Stoeckli-Evans, H. *J. Am. Chem. Soc.* **2003**, *125*, 14046.

(8) (a) Yoo, J.; Yamaguchi, A.; Nakano, M.; Krystek, J.; Streib, W. E.; Brunel, L. C.; Ishimoto, H.; Christou, G.; Hendrickson, D. N. *Inorg. Chem.* **2001**, *40*, 4604. (b) Hendrickson, D. N.; Christou, G.; Ishimoto, H.; Yoo, J.; Brechin, E. K.; Yamaguchi, A.; Rumberger, E. M.; Aubin, S. M. J.; Sun Z.; Aromí, G. *Polyhedron* **2001**, *20*, 1479. (c) Yang, E. C.; Harden, N.; Werndorfer, W.; Zakhrov, L.; Brechin, E. K.; Rheingold, A. L.; Christou G.; Hendrickson, D. N. *Polyhedron* **2003**, *22*, 1857;

(9) Lecren, L.; Li, Y.-G.; Wernsdorfer, W.; Roubeau, O.; Miyasaka, H.; Clérac, R. *Inorg. Chem. Commun*. **2005**, *8*, 626.

(10) Miyasaka, H.; Nakata, K.; Sugiura, K.; Yamashita, M.; Clérac, R. *Angew. Chem., Int. Ed.* **2004**, *43*, 707.

(11) Yoo, J.; Wernsdorfer, W.; Yang, E.-C.; Nakano, M.; Rheingold, A. L.; Hendrickson, D. N. *Inorg. Chem.* **2005**, *44*, 3377.

(40 mL, bis(2-methoxyethyl)ether) in a narrow glass tube, and left to stand for several days to form brown rectangular crystals of **1**. Yield: 86 mg, 29% (based on Mn). Selected IR (KBr): ν 2264 (s), 2210 (s), 2154 (s), 1606 (s), 1569 (w), 1471 (w), 1438 (m), 1384 (s), 1342 (w), 1309 (w), 1296 (w), 1226 (w), 1157 (w), 1045 (s), 819 (w), 759 (s), 719 (w), 675 (m) cm^{-1}. Anal. Calcd for $C_{44}H_{42}Mn_4N_{16}O_{12}$ (**1**): C, 43.80; H, 3.51; N, 18.57. Found: C, 43.31; H, 3.52; N, 18.50.

Synthesis of $[Mn_4(hmp)_4(Hpdm)_2(dcn)_2](ClO_4)_2\cdot 2H_2O\cdot 2MeCN$ (2). To an acetonitrile solution (40 mL) of manganese perchlorate hexahydrate (724 mg, 2 mmol) was added 2-hydroxymethylpyridine (546 mg, 5 mmol) and 20 wt % water solution of tetraethylammonium hydroxide (1.472 g, 2 mmol). After stirring for 1 h, solids of both pyridine-2,6-dimethanol (139 mg, 1 mmol) and sodium dicyanamide (89 mg, 1 mmol) were added to the solution that was then further stirred for 1 h. The resulting solution was filtered, carefully layered on diglyme (80 mL) in a narrow glass tube, and left to stand for several days to form red-brown rectangular crystals of **2**. Yield: 435 mg, 63% (based on Mn). Selected IR (KBr): ν 2301 (s), 2239 (s), 2166 (s), 1605 (s), 1580 (m), 1568 (w), 1481 (m), 1441 (s), 1358 (s), 1283 (m), 1227 (w), 1045 (s), 930 (w), 826 (w), 773 (s), 719 (m), 671 (s), 625 (s), 577 (s), 540 (m), 515 (m) cm^{-1}. Anal. Calcd for $C_{46}H_{50}Cl_2Mn_4N_{14}O_{18}$ (**2**): C, 40.10; H, 3.66; N, 14.23. Found: C, 40.70; H, 3.64; N, 14.58.

Synthesis of $[Mn_4(hmp)_4Br_2(OMe)_2(dcn)_2]\cdot 0.5H_2O\cdot 2THF$ (3). A methanol solution (5 mL) containing $[Mn_4(hmp)_6Br_2(H_2O)_2]Br_2$, 52 mg (0.04 mmol) and sodium dicyanamide 7 mg (0.08 mmol) was stirred for 1 h at room temperature. The resulting solution was filtered, carefully layered on tetrahydrofuran (10 mL) in a narrow glass tube, and left to stand for several days to form brown rectangular crystals of **3**. Yield: 29 mg, 62% (based on Mn). Selected IR (KBr): ν 2303 (m), 2239 (m), 2168 (s), 1609 (s), 1570 (w), 1483 (m), 1439 (s), 1364 (m), 1285 (m), 1227 (w), 1155 (w), 1067 (s), 1047 (s), 825 (w), 764 (m), 719 (w), 671 (m), 572 (m), 523 (m) cm^{-1}. Anal. Calcd for $C_{38}H_{47}Br_2Mn_4N_{10}O_{8.5}$ (**3**): C, 39.37; H, 4.09; N, 12.08. Found: C, 39.69; H, 4.32; N, 11.93.

Synthesis of $[Mn_4(hmp)_6(dcn)_2](ClO_4)_2$ (4). To an acetonitrile solution (20 mL) of manganese perchlorate hexahydrate (499 mg, 1.38 mmol) was added 2-hydroxymethylpyridine (379 mg, 3.47 mmol) and 20 wt % water solution of tetraethylammonium hydroxide (531 mg, 0.72 mmol). After stirring for 1 h, sodium dicyanamide (51 mg, 0.57 mmol) was added to the solution that was then further stirred 1 h. The resulting solution was filtered, carefully layered on diglyme (40 mL) in a narrow glass tube, and left to stand for several days to form red-brown rectangular crystals of **4**. Yield: 242 mg, 58% (based on Mn). Selected IR (KBr): ν 2314 (s), 2235 (s), 2168 (s), 1607 (s), 1572 (m), 1485 (s), 1462 (m), 1441 (s), 1385 (s), 1366 (s), 1285 (m), 1223 (w), 1157 (m), 1089 (s), 1045 (s), 920 (w), 824 (m), 766 (s), 729 (m), 675 (s), 660 (s), 623 (s) cm^{-1}. Anal. Calcd for $C_{40}H_{36}Cl_2Mn_4N_{12}O_{14}$ (**4**): C, 40.05; H, 3.03; N, 14.01. Found: C, 40.04; H, 3.18; N, 14.12.

Physical Measurements. Infrared spectra were measured on KBr disks with a Shimadzu FT-IR-8600 spectrophotometer. Magnetic susceptibility measurements were obtained with the use of a Quantum Design SQUID magnetometer MPMS-XL. Direct current (dc) measurements were collected from 1.8 to 300 K and from −70 to 70 kOe. Alternate current (ac) measurements were performed at various frequencies from 1 to 1488 Hz with ac field amplitude of 3 Oe. The freshly synthesized samples of **1**−**4** were used for each magnetic measurement to avoid deterioration of the crystal samples, and the measurements were performed using finely ground polycrystalline samples restrained by *n*-eicosane or Nujol. The experimental data were also corrected for the sample holder, for the resin, and for the diamagnetic contribution calculated from Pascal constants.[12] Heat capacities were measured on a single crystal (147.4 μg for **1**, 61.9 μg for **2**, 90.0 μg and 83.5 μg for **3**, 126.7 μg for **4**) by a thermal relaxation technique in a ^{3}He cryostat (lowest temperature: 0.4 K). In each measurement, the blank heat capacity including a small amount of Apiezon N grease (less than 1 mg) used for adhesion was measured prior to the sample mounting. The heat capacities are determined by subtracting the blank data fitted by polynomials from the measured total heat capacities.

Crystallography. Single crystals of **1**−**4** used for X-ray crystallography were prepared by the methods described in the synthetic procedure and mounted on a glass rod (crystal dimensions: 0.15 mm × 0.25 mm × 0.25 mm for **1**, 0.15 mm × 0.20 mm × 0.20 mm for **2**, 0.05 mm × 0.15 mm × 0.15 mm for **3**, and 0.25 mm × 0.25 mm × 0.25 mm for **4**). Data collections were made on a Rigaku CCD diffractometer (Saturn 70) with graphite monochromated Mo Kα radiation ($\lambda = 0.71069$ Å). The structures were solved by a direct method (SIR92)[13] and expanded using Fourier techniques.[14] Non-hydrogen atoms were refined anisotropically, while hydrogen atoms were introduced as fixed contributors. Full-matrix least-squares refinements on F^2 based on 7087 for **1**, 8538 for **2**, 7026 for **3**, and 12769 for **4** unique reflections were employed, where the unweighted and weighted agreement factors of R1 $= R = \sum||F_o| - |F_c||/\sum|F_o|$ ($I > 2.00\sigma(I)$ for R1 and all data for R), and wR2 $= [\sum w(F_o^2 - F_c^2)^2/\sum w(F_o^2)^2]^{1/2}$ (all data) were used. A Sheldrick weighting scheme was used. Plots of $\sum w(F_o^2 - F_c^2)^2$ versus F_o^2, reflection order in data collection, sin θ/λ and various classes of indices showed no unusual trends. Neutral atom scattering factors were taken from Cromer and Waber.[15] Anomalous dispersion effects were included in F_{calcd}; $\Delta f'$ and $\Delta f''$ were from Creagh and McAuley.[16] The mass attenuation coefficients were from Creagh and Hubbell.[17] All calculations were performed using the CrystalStructure crystallographic software package.[18] Crystallographic data for the four compounds are summarized in Table 1.

Results and Discussion

Syntheses and General Structural Comments. Mixed-valence double-cuboidal $[Mn_4]$ complexes can be easily obtained from Mn^{II} salts in the combination with a chelating−bridging ligand such as Hhmp or Hpdm and an organic base (NEt_4OH). The $[Mn_4]$ core of these complexes is composed of two Mn^{II} and two Mn^{III} ions. Their oxidation states can be easily assigned as trivalent and divalent for respectively the inner and outer manganese sites based on charge balance consideration, bond valence sum calculation,[19] and Jahn Teller distortion on the Mn^{III} site. Indeed, a few compounds of this family have been reported to date with the hmp$^-$,[5d,8,9] pdm^{2-},[8b,20a,b] and triethanolamine ligands.[20c] In the past few years, we have been studying the new manganese complexes based on the hmp$^-$ ligand and the synthetic strategy to control the versatile chemistry of this

---

(12) Boudreaux, E. A., Mulay, L. N., Eds. *Theory and Applications of Molecular Paramagnetism*; John Wiley & Sons: New York, 1976.

(13) SIR92: Altomare, A.; Burla, M. C.; Camalli, M.; Cascarano, M.; Giacovazzo, C.; Guagliardi, A.; Polidori, G. *J. Appl. Crystallogr.* **1994**, *27*, 435.

(14) DIRDIF94: Beurskens, P. T.; Admiraal, G.; Beurskens, G.; Bosman, W. P.; de Gelder, R.; Israel, R.; Smits, J. M. M. 1994.

(15) Cromer, D. T.; Waber, J. T. *International Tables for Crystallography*; The Kynoch Press: Birmingham, England, 1974; Vol. IV, Table 2.2A.

(16) Creagh, D. C.; McAuley, W. J. In *International Tables for Crystallography*; Wilson, A. J. C., Ed.; Kluwer Academic Publishers: Boston, 1992; Vol. C, Table 4.2.6.8, pp 219−222.

(17) Creagh, D. C.; Hubbell, J. H. In *International Tables for Crystallography*; Wilson, A. J. C., Ed.; Kluwer Academic Publishers: Boston, 1992; Vol. C, Table 4.2.4.3, pp 200−206.

(18) CrystalStructure 3.15: *Crystal Structure Analysis Package*; Rigaku and Rigaku/MSC: 9009 New Trails Dr., The Woodlands, TX 77381, U.S.A., 2000−2002.

(19) Brown, I. D.; Altermatt, D. *Acta Crystallogr. B* **1985**, *41*, 244.

(20) (a) Brechin, E. K.; Yoo, J.; Nakano, M.; Huffman, J. C.; Hendrickson, D. N.; Christou, G. *Chem. Commun.* **1999**, *17*, 783. (b) Yoo, J.; Brechin, E. K.; Yamaguchi, A.; Nakano, M.; Huffman, J. C.; Maniero, A. L.; Brunel, L.-C.; Awaga, K.; Ishimoto, H.; Christou, G.; Hendrickson, D. N. *Inorg. Chem.* **2000**, *39*, 3615. (c)Wittick, L. M.; Murray, K. S.; Moubaraki, B.; Batten, S. R.; Spiccia, L.; Berry, K. *J. Chem. Soc. Dalton Trans.* **2004**, 1003.

Table 1. Crystallographic Data for **1**−**4**

	1	**2**	**3**	**4**
formula	$C_{44}H_{42}Mn_4N_{16}O_{12}$	$C_{46}H_{50}Cl_2Mn_4N_{14}O_{18}$	$C_{38}H_{47}Br_2Mn_4N_{10}O_{8.5}$	$C_{40}H_{36}Cl_2Mn_4N_{12}O_{14}$
formula weight	1206.67	1377.64	1159.41	1199.45
color, shape	brown, prism	brown, prism	brown, prism	brown, prism
crystal system	monoclinic	monoclinic	monoclinic	orthorhombic
space group	$P2_1/n$ (No. 14)	$C2/c$ (No. 15)	$C2/c$ (No. 15)	$P2_12_12_1$ (No. 19)
a/Å	11.151(3)	28.322(8)	20.76(2)	14.530(3)
b/Å	10.043(2)	11.093(3)	11.688(7)	16.999(3)
c/Å	23.047(5)	20.207(6)	21.196(14)	18.440(3)
α/deg	90	90	90	90
β/deg	102.570(2)	111.754(3)	107.884(9)	90
γ/deg	90	90	90	90
V/Å^3	2519.4(10)	5897(3)	4895(7)	4554.4(13)
T/°C	−180(1)	−155(1)	−160(1)	−180(1)
Z	2	4	4	4
D_{calc}/g·cm^{-3}	1.591	1.552	1.573	1.749
F_{000}	1228	2808	2332	2424
λ/Å	0.71070	0.71070	0.71070	0.71070
μ (Mo Kα)/cm^{-1}	10.57	10.07	27.03	12.83
data measured	5624	7196	5552	11085
data unique	7087	8538	7026	12769
R_{int}	0.061	0.032	0.023	0.039
no. of observations ($I > 2.00\sigma(I)$)	4398	5152	4291	7950
no. of variables	364	404	289	686
GOF	1.027	1.290	1.079	1.000
R1^a($I > 2.00\sigma(I)$))	0.030	0.067	0.064	0.027
R, wR2^b(all data)	0.038, 0.079	0.073, 0.177	0.068, 0.176	0.034, 0.060

[a] $R1 = \sum||F_o| - |F_c||/\sum|F_o|$. [b] $wR2 = [\sum w(F_o^2 - F_c^2)^2/\sum w(F_o^2)^2]^{1/2}$.

system. For these compounds, the coordination sphere of the Mn^{III} ions is occupied by two hmp^- ligands and two L^1 ligands as shown in Scheme 1b. The alkoxo groups of these two species bridge each Mn^{III} to its neighbor Mn^{III} and Mn^{II} ions through μ-oxygen and μ_3-oxygen bridging modes. When a noncoordinatable counteranion is used, available coordination sites on the outer Mn^{II} ions (i.e., terminal positions) are occupied by solvent molecules as illustrated in the perchlorate complex, $[Mn_4(hmp)_6(CH_3CN)_2(H_2O)_4](ClO_4)_4·2CH_3CN$, in which the terminal positions are occupied by the acetonitrile and water molecules.[9a] On the other hand, a coordinatable counteranion can be introduced during the reaction either directly by the corresponding Mn^{II} salt or by an additional reactant (e.g., sodium or silver salt). In this case, the available sites on the Mn^{II} ions are partially or totally occupied by these anions as exemplified by $[Mn_4(hmp)_6(MeCN)_2(NO_3)_2](ClO_4)_2·4MeCN$,[8c] $[Mn_4(hmp)_6(NO_3)_4]·MeCN$,[8c] or $[Mn_4(hmp)_6(H_2O)_2(NO_3)_2](NO_3)_2·2.5H_2O$[5d] that possess the terminal coordinating nitrato anions. Note that $[Mn_4(hmp)_6(H_2O)_2Br_2](Br)_2·4H_2O$[8a,b] and $[Mn_4(hmp)_4(MeO)_2(acac)_2](ClO_4)_2·4MeOH$[8c] also illustrate the same idea with the bromide and acetylacetonate (acac) anions. As expected, the core of the $[Mn_4]$ cluster remains quasi-identical in this family of compound, although the external (terminal) coordination sites on the Mn^{II} ions have been dramatically modified as mentioned above. Therefore, this coordination ability confers high flexibility to these SMM molecules that can act as building blocks to construct new magnetic architectures by using appropriate polydentate bridging ligands. In this vein, Hendrickson et al. have shown very recently the chloride-bridged 1D compound, $[Mn_4(hmp)_6Cl_2](ClO_4)_2$.[11] In our group, we have investigated the versatility of this system in the presence of dicyanamide anions ($N(CN)_2^-$ hereafter abbreviated as dcn^-) in order to connect the $[Mn_4]$ units into extended structures. The dicyanamide anion acts, in many cases, as a linear-type bidentate bridging ligand ($\mu_{1,5}$-bridging mode) with divalent first-row transition metals (note that the monodentate or tridentate coordination modes have also been observed).[21] As mentioned in the Introduction, we have reported in 2004 on the first network compound, $[Mn_4(hmp)_4(\mu_3\text{-}OH)_2][Mn^{II}(dcn)_6]·2MeCN·THF$, involving the covalently linked dcn^- ligand and $[Mn_4]$ units.[10] This compound was obtained in a one-pot assembly reaction in a basic MeCN/THF solution that contained $Mn(ClO_4)_2·6H_2O$, hmp^-, and Na(dcn) in a 1:2:1 molar ratio, respectively. In this material, the three available sites on the Mn^{II} ions of the $[Mn_4]$ unit are all occupied by the dcn^- ligands that bind in the $\mu_{1,5}$ mode to a Mn^{II} ion (forming the $[Mn^{II}(dcn)_6]^{4-}$ unit) to develop a 3D coordination network.[10] Using the same synthetic conditions as for this compound but starting from the $Mn(NO_3)_2·6H_2O$ precursor, the discrete complex **1**, $[Mn_4(hmp)_6(NO_3)_2(dcn)_2]·2MeCN$, was obtained. Indeed, this result is not surprising as we previously observed that the NO_3^- anions possess the strong affinity to coordinate to the Mn^{II} sites of the $[Mn_4]$ core (vide supra). Thus, these NO_3^- anions prevent to trap more than two dcn^- ligands on the $[Mn_4]$ unit.

Then, it was interesting for us to try to control the structural dimensionality of the resulting compound by playing on the synthetic conditions of the $[Mn_4]/dcn^-$ system. For this purpose, three different approaches have been used. First, maintaining the one-pot synthesis used for the 3D compound, we have played on the chemical stoichiometry of the reaction. When the molar ratio $Mn(ClO_4)_2·6H_2O$: Hhmp: Na(dcn) is adjusted to 1:2.5:0.4, we obtained $[Mn_4(hmp)_6(dcn)_2](ClO_4)_2$ (**4**) in relatively good yield. In comparison to the 3D compound, the higher $hmp^-:dcn^-$ ratio induced the formulation with only four dcn^- anions for the $[Mn_4]$ unit that preserves its six hmp^- ligands. The formula of **4** clearly shows that the reduction of the dcn^-

---

(21) Batten, S. R.; Murray, K. S. *Coord. Chem. Rev.* **2003**, *246*, 103.

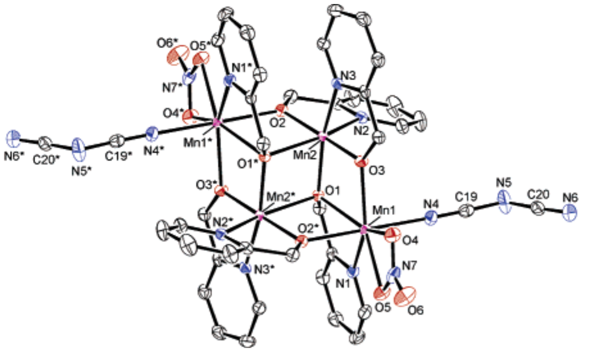

Figure 1. ORTEP drawing of the $[Mn_4]$ unit in **1** with atomic numbering scheme for selected atoms (50% probability thermal level), where symmetry operation (*): $-x + {}^1/_2, -y + {}^3/_2, -z + 1$. Hydrogen atoms are omitted for clarity.

coordination number is directly responsible for the stabilization of a 2D network (vide infra).

Another way to reduce the coordination number of dcn^- on the Mn^{II} sites is to use a co-ligand with an additional coordination function in comparison to hmp^-. Thus, as the second approach, we chose the use of the H_2pdm ligand as the co-ligand (see Scheme 1a), which possesses the second $-CH_2OH$ group as the monoanionic form, $Hpdm^-$. Using the ratio $Mn(ClO_4)_2 \cdot 6H_2O$: Hhmp: H_2pdm : Na(dcn) adjusted to 1:2.5:0.5: 0.5, we obtained $[Mn_4(hmp)_4(Hpdm)_2(dcn)_2](ClO_4)_2 \cdot 2H_2O \cdot 2MeCN$ (**2**) that also has a 2D arrangement of the $[Mn_4]$ units. The $Hpdm^-$ co-ligand has played its role replacing two hmp^- ligands on the prototype $[Mn_4]$ cores and blocking one coordination position on the Mn^{II} sites by the second $-CH_2OH$ group of $Hpdm^-$. This coordination mode allowed consequently the presence of only four dcn^- ligands on the $[Mn_4]$ unit as observed for **4**.

Finally, we also explored the possibility of using a two-step reaction involving the pre-isolation of the $[Mn_4]$ complex followed by the reaction of this species with dcn^-. Therefore, we first synthesized the known $[Mn_4(hmp)_6Br_2(H_2O)_2]Br_2 \cdot 4H_2O$ complex[8] (see Experimental Section) as the $[Mn_4]$ precursor and then reacted it with Na(dcn) in a 1:2 ratio. The two water molecules, but also more surprisingly two hmp^- ligands, have been replaced by four dcn^- anions, leading to $[Mn_4(hmp)_4Br_2(OMe)_2(dcn)_2] \cdot 0.5H_2O \cdot 2THF$ (**3**). As well as **2** and **4**, the presence of these four dcn^- ligands leads to a 2D organization. In summary, the $[Mn_4]/dcn^-$ system appears very versatile, but its chemistry can be rationalized by a fine-tuning of the synthetic conditions. As shown by this work, the double cuboidal $[Mn_4]$ unit (Scheme 1b) is always preserved in the whole family of compounds, although the Mn^{II} coordination sphere is strongly modified (by L^1 and L^2 ligands in Scheme 1b). The chemical control of the coordination number of the dcn^- ligand on the Mn^{II} ions has been the key to obtain discrete cluster (**1**), 2D networks (**2**, **3**, and **4**), but also the previously reported 3D architecture.[10]

Structural Description of 1. Compound **1**, crystallizing in monoclinic space group $P2_1/n$ ($Z = 2$), has an inversion center at the center of $[Mn_4]$ core (the midpoint of Mn(2)···Mn(2*), Figure 1). The selected bond distances and angles are summarized in Table 2 with other compounds presented herein.

While the inner Mn^{III} ions are hexacoordinated (common fashion through the compounds of this family), each outer Mn^{II} ion is heptacoordinated by two alkoxy oxygen atoms (μ-O(2) and −O(3)) of the neighboring hmp^- ligands chelating the inner Mn^{III} ions, one bidentate hmp^-, one NO_3^- as the bidentate ligand, and one dicyanamide as the terminal unidentate ligand (Figure 1). The Jahn−Teller axis at the Mn(2) sites is assigned to the average [N(2)−Mn(2)−O(1)*] axis as indicated by the significantly longer bond distances of N(2)−Mn(2) = 2.1995(17) Å and O(1)*−Mn(2) = 2.2458(14) Å compared with the bond distances in the equatorial plane [an average bond distance: 1.9431 Å]. The two Jahn−Teller axes on Mn(2) and Mn(2)* are parallel to each other. The N(2)−Mn(2)−O(1)* angle is slightly bent reaching 157.73(6)° as already observed for example in $[Mn_4(hmp)_4(\mu_3\text{-}OH)_2][Mn^{II}(dcn)_6] \cdot 2MeCN \cdot THF$ (159.6(1)°)[10] or $[Mn_4(hmp)_6Br_2(H_2O)_2]Br_2 \cdot 4H_2O$ (158°).[8a] As expected for typical Mn^{II} ions, the bond distances around the heptacoordinated Mn(1) site are significantly longer than those at the Mn^{III} site [an average bond distance: 2.2573 Å]. It is worth noting that the nearest intermetallic distance between these discrete $[Mn_4]$ complexes is about 7.54 Å and that no weak intercomplex interactions, such as $\pi-\pi$ stacking or hydrogen bonding, are found.

Structural Description of 2. Compound **2** crystallizes in monoclinic space group $C2/c$ ($Z = 4$) with an inversion center at the center of $[Mn_4]$ core (the midpoint of Mn(2)···Mn(2*)). As shown in Figure 2, the two inner Mn^{III} ions of the double-cuboidal $[Mn_4]$ core are hexacoordinated, while outer Mn^{II} ions are heptacoordinated. The coordination geometry around the Mn(2) ion is essentially the same as in **1**. Nevertheless in **2**, two $Hpdm^-$ ligands replace the two hmp^- (as L^1 in Scheme 1b) present in **1**, and hence, each of them gives one of its alkoxy oxygen atoms to form a central μ_3-O(1) bridge. The coordination sphere of the outer Mn(1) ion is occupied by the chelating $Hpdm^-$ (as L^1) (pyridine, the μ_3-O(1) alkoxy oxygen atom and

Table 2. Selected Bond Distances (Å) and Angles (deg°) for **1**−**4** (See Structural Definition Given in Scheme 1b)

	1	2	3	4
$Mn^{II}-(\mu_3\text{-}O)$	2.2816(14)	2.373(3)	2.301(3)	2.262(2)−2.265(2)
$Mn^{II}-(\mu\text{-}O)$	2.1920(14)−2.2115(14)	2.219(2)−2.246(2)	2.182(3)−2.196(3)	2.159(2)−2.242(2)
$Mn^{II}-N_{L1}$	2.2769(18)	2.316(3)		2.208(3)−2.239(2)
$Mn^{II}-L^2$	2.2996(16)−2.3370(16)	2.294(4)	2.5676(10)	
$Mn^{II}-N_{N(CN)2}$	2.2025(19)	2.222(3)−2.227(4)	2.192(4)−2.197(5)	2.117(2)−2.217(2)
$Mn^{III}-(\mu_3\text{-}O)$	1.9727(14)	1.964(2)	2.063(3)	1.970(2)−2.243(2)
$Mn^{III}-(\mu\text{-}O)$	1.8686(15)−1.8768(14)	1.860(3)−1.890(3)	1.872(4)−1.869(3)	1.866(2)−1.885(2)
$Mn^{III}-N_{hmp}$	2.0542(19)	2.061(3)	2.107(4)	2.045(2)−2.067(2)
$Mn^{III}-(\mu_3\text{-}O)$ (Jahn−Teller axis)	2.2458(14)	2.239(2)	2.133(3)	2.231(2)−2.243(2)
$Mn^{III}-N_{hmp}$ (Jahn−Teller axis)	2.1995(17)	2.222(3)	2.153(3)	2.200(2)−2.209(2)
$Mn^{II}-(\mu\text{-}O)-Mn^{III}$	108.06(7)−109.84(6)	109.06(13)−111.05(14)	109.10(16)−109.69(14)	106.25(10)−109.12(10)
$Mn^{II}-(\mu_3\text{-}O)-Mn^{III}$	95.49(5)−101.14(6)	94.67(12)−100.78(12)	97.23(12)−98.40(14)	95.42(7)−99.73(9)
$Mn^{III}-(\mu_3\text{-}O)-Mn^{III}$	98.91(5)	100.60(11)	97.71(13)	98.19(8)−98.61(9)

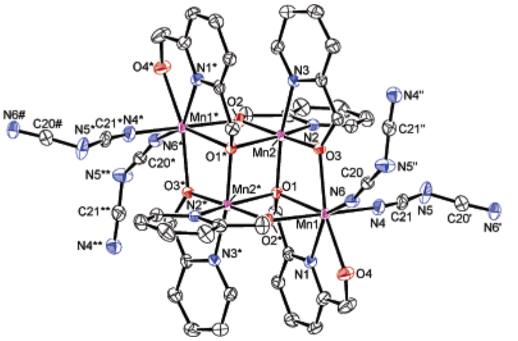

Figure 2. ORTEP drawing of the $[Mn_4]$ unit in **2** with atomic numbering scheme for selected atoms (50% probability thermal level), where symmetry operations (*): $-x + {}^1/_2, -y + {}^3/_2, -z + 1$; (**): $+x, -y + 1, z + {}^1/_2$; (#): $+x, -y + 2, +z + {}^1/_2$; (′): $-x + {}^1/_2, +y - {}^1/_2, -z + {}^1/_2$; (″): $-x + {}^1/_2, +y + {}^1/_2, -z + {}^1/_2$. Hydrogen atoms are omitted for clarity.

the alcohol group of $Hpdm^-$), two dicyanamide ligands, and two alkoxy oxygen atoms, μ-O(2) and -O(3) of the hmp^- ligands that chelate the inner Mn^{III} ions (Figure 2). Note that the position of H atom of $Hpdm^-$ was not directly identified experimentally but should be located on the O4 atom because of the formation of hydrogen bond with the ClO_4^- counteranions ($O4\cdots O_{ClO4^-} = 2.768(5)$ Å).

As expected for the Mn^{III} ions, the Jahn−Teller distortion is observed on the Mn(2) site along the average N(2)−Mn(2)−O(1)* direction. In the equatorial plane, significantly shorter bond distances are found [an average bond distance: 1.9438 Å] than the bond distances in the axial positions: N(2)−Mn(2) = 2.222(3) Å and O(1)*−Mn(2) = 2.239(2) Å. The two mean Jahn−Teller axes on the Mn(2) sites are parallel to each other, while the N(2)−Mn(2)−O(1)* angle is slightly bent [159.88(14)°]. The average bond distance on Mn(1) is 2.2710 Å as expected for the divalent Mn ion.

The two dcn^- ligands act as a bidentate bridging ligand in **2**. Indeed, they link covalently the Mn(1) ions of the neighboring $[Mn_4]$ units, forming a 2D network running in the *bc* plane, as shown in Figure 3. Two different orientations of the $[Mn_4]$ complexes are found in the same layer. This organization thus induces the presence of two $[Mn_4]$ Jahn−Teller axis orientations with a splitting angle of about 80°. The Mn···Mn distances within the layer are 8.2044 and 8.1721 Å via the dcn^- bridge and through space, respectively, whereas the nearest interlayer Mn···Mn distance is 10.8148 Å. The counter ClO_4^- anions and interstitial solvents (MeCN and H_2O molecules) occupy the void space between the layers.

Structural Description of 3. Compound **3** crystallizes in monoclinic space group *C*2/*c* (*Z* = 4) with an inversion center at the midpoint of Mn(2)···Mn(2*). The rhombic $[Mn_4]$ core observed in **3** (Figure 4) is similar to that observed in **1** and **2**, although this time, all four Mn ions are hexacoordinated, while the outer Mn^{II} ions were heptacoordinated in **1** and **2**.

The inner Mn(2) ion is chelated by two hmp^- ligands in a cis fashion and interconnected by two methoxy O(3) bridges (as L^1 in Scheme 1b) to form a $[(hmp)_2Mn(2)-(OMe)_2-Mn(2)(hmp)_2]$ motif. To form the recurrent $[Mn_4]$ core, this unit is connected to the two outer Mn(1) centers by the two methoxy oxygen atoms (μ_3-O(3)) and alkoxy oxygen atoms (μ-O(2) and -O(3)) of hmp^- chelating the Mn(2) ions (Figure 4). The octahedral coordination sphere around the Mn(1) ion completed by two other types of ligands, the terminal Br(1) anion and two dcn^- ligands. As expected, the bond distances around the Mn(1) site are typical for a Mn^{II} ion with an average value of 2.273 Å. Around the Mn(2) site, the N(2)−Mn(2) = 2.153(3) Å and O(1)*−Mn(2) = 2.133(3) Å bond distances corresponding to the axial positions are significantly longer than the bond

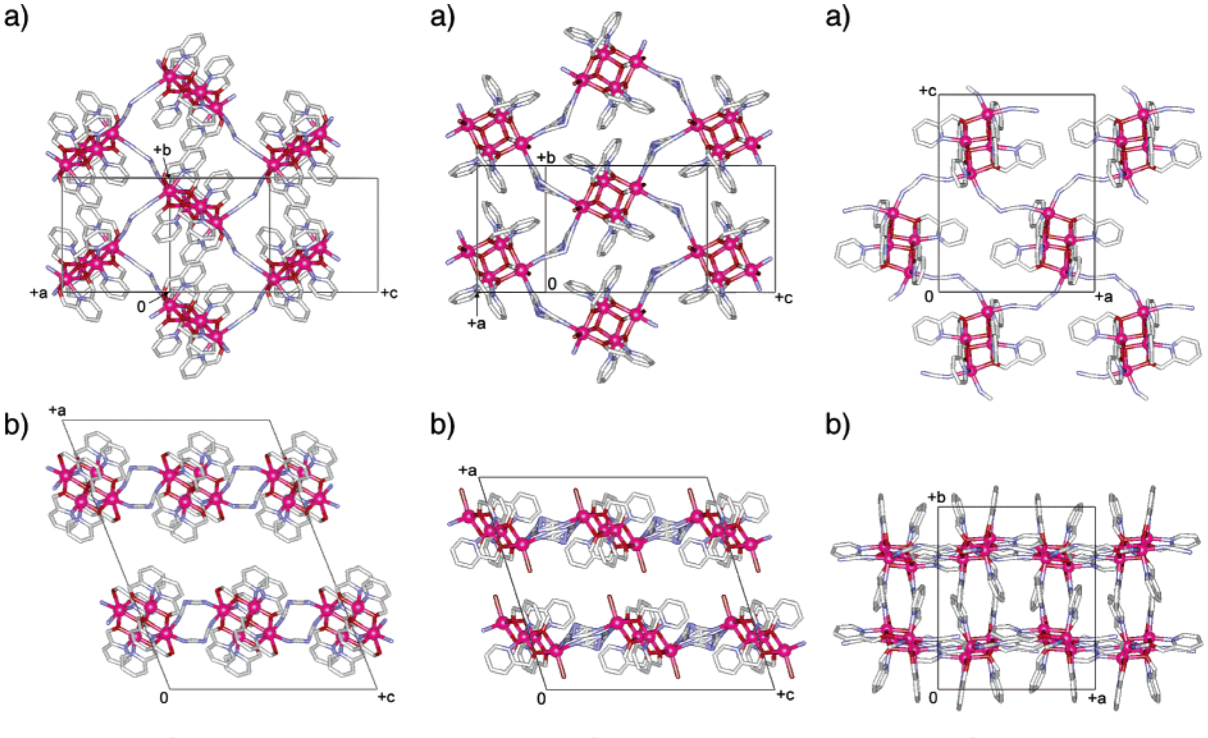

Comp. 2 **Comp. 3** **Comp. 4**

Figure 3. Packing diagrams of **2**−**4**. For **2**, (a) the projection along the *a** axis and (b) the projection along the *b* axis. For **3**, (a) the projection along the *a** axis and (b) the projection along the *b* axis. For **4**, (a) the projection along the *b* axis and (b) the projection along the *c* axis.

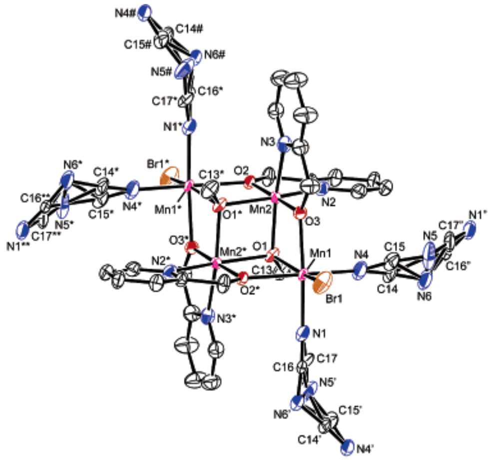

Figure 4. ORTEP drawing of the [Mn$_4$] unit in **3** with atomic numbering scheme for selected atoms (50% probability thermal level), where symmetry operations (*): $-x + {}^1/_2$, $-y + 1$, $-z$; (**): $+x$, $-y$, $+z + {}^1/_2$; (#): $+x$, $-y + 1$, $+z + {}^1/_2$; ($'$): $-x + {}^1/_2$, $+y - {}^1/_2$, $-z - {}^1/_2$; ($''$): $-x + {}^1/_2$, $+y + {}^1/_2$, $-z - {}^1/_2$. Hydrogen atoms are omitted for clarity.

distances composing the equatorial plane [an average bond distance: 1.9778 Å]. Hence, the average N(1)−Mn(2)−O(3)* axis (the N(2)−Mn(2)−O(3)* angle is 160.93(17)°) corresponds to the Jahn−Teller axis of the Mn(2) site (the two Jahn−Teller axes of the [Mn$_4$] core are parallel to each other). The N(CN)$_2^-$ bridging ligands exhibit a strong disorder (Figure 4) as already seen in such $\mu_{1,5}$ bidentate coordination modes (the sets of C14 and C15, C16 and C17, and N5 and N6 in Figure 4 are disordered and thermally populated within the sum of the occupancy of 1.0).[21,22] These dcn$^-$ ligands bridge covalently the Mn(1) ions of neighboring [Mn$_4$] units and induce a 2D arrangement of the [Mn$_4$] units running in the *bc* plane, as shown in Figure 3. Two different orientations of the [Mn$_4$] complexes are found in the same layer. This organization thus induces the presence of two [Mn$_4$] Jahn−Teller axis orientations that are lying in a plane perpendicular to the *a* axis with a splitting angle of about 63°. The Mn···Mn distances within the layer are 8.549 and 8.770 Å via the dcn$^-$ bridges and through space, respectively. Between the layers, tetrahydrofuran and water molecules are located as interstitial solvents, and lead to the nearest interlayer Mn···Mn distance of 8.546 Å. It is worth noting that the intra- and interlayer Mn···Mn distances are slightly longer and much shorter, respectively, than those in **2**.

Structural Description of 4. Compound **4** crystallizes in orthorhombic space group $P2_12_12_1$ ($Z = 4$). An ORTEP drawing of **4** is depicted in Figure 5 and the selected bond distances and angles are summarized in Table 2. Similarly to **3**, the double-cuboidal [Mn$_4$] unit of **4** contains only hexacoordinated Mn ions. The coordination sphere of the outer Mn^{II} ions is occupied by pyridine (N(1) or N(4)) and alkoxy (μ_3-O(1) or -O(4)) groups coming from the hmp$^-$ ligands, a set of alkoxy groups (μ-O(3) and -O(5) or μ-O(2) and -O(6)) carried by the hmp$^-$ ligands chelating the inner Mn^{III} ions, and finally two dcn$^-$ anions.

The coordination geometry around Mn(2) and Mn(3) has the Jahn−Teller distortion with an elongated axis along the average [N(2)−Mn(2)−O(4)] and [N(5)−Mn(3)−O(1)] directions [N(2)−Mn(2) = 2.209(2) Å and O(4)−Mn(2) = 2.231(2) Å; N(5)−Mn(3) = 2.200(2) Å and O(1)−Mn(3) = 2.243(2) Å]. The N(2)−Mn(2)−O(4) and N(5)−Mn(3)−O(1) axes are bent at 160.29(9)° and 160.79(9)°, respectively. In the equatorial plane of the Mn^{III} ions, an average bond distance is 1.9495 Å for Mn(2) and 1.9415 Å for Mn(3). The bond distances around the Mn(1) and Mn(4) sites are significantly longer than the bond distances at the Mn(2) and Mn(3) sites, confirming their divalent nature. The bidentate dcn$^-$ ligands link covalently the Mn(1) and Mn(4) ions of neighboring [Mn$_4$] units to form a 2D network running in the *ac* plane, as shown in Figure 3. This organization and the symmetry of the structure induce the presence of two [Mn$_4$] complex orientations within the same layer. The resulting two Jahn−Teller axes are approximately lying on the *ac* plane and orientated at about ±9° from the *a* axis. The Mn···Mn distance via the dcn$^-$ bridge is 8.161 Å, whereas the only presence of counteranions (ClO$_4^-$) between the layers leads to nearest interlayer Mn···Mn distance of 8.587 Å. It is interesting to comment that between the sheets the benzene rings of hmp$^-$ make $\pi-\pi$ stacking with C···C distances of ~3.43 Å (Figure 3).

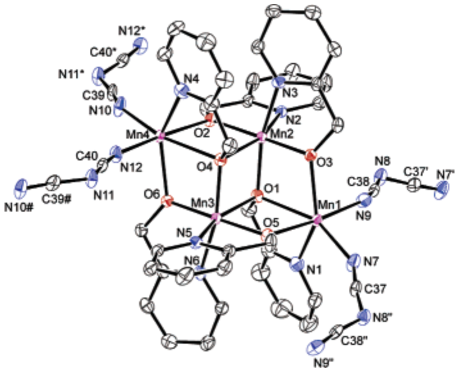

Figure 5. ORTEP drawing of the [Mn$_4$] unit in **4** with atomic numbering scheme for selected atoms (50% probability thermal level), where symmetry operations (*): $+x - {}^1/_2$, $-y + {}^1/_2$, $-z$; (#): $+x + {}^1/_2$, $-y + {}^1/_2$, $-z$; ($'$): $+x - {}^1/_2$, $-y + {}^1/_2$, $-z + 1$; ($''$): $+x + {}^1/_2$, $-y + {}^1/_2$, $-z + 1$. Hydrogen atoms are omitted for clarity.

High-Temperature Magnetic Properties of 1−4. Compounds **1**−**4** present a very similar behavior already observed for this type of [Mn$_4$] complexes.[5d,8,9] The temperature dependence of χT products of **1**−**4** are shown in Figure 6. The χT increases upon lowering temperature from about 16 cm^3·K·mol^{-1} at 300 K (in good agreement with the expected value for uncoupled Mn^{II} and Mn^{III} ions, i.e., 14.75 cm^3·K·mol^{-1} for $g = 2$), to a maximum of 39.1/37.2/33.7/29.7 cm^3·K·mol^{-1} at T_{max} = 7.0/4.3/13.0/16.0 K for **1**, **2**, **3**, and **4**, respectively. This χT increasing behavior is induced by a set of ferromagnetic interactions, J_{bb} between the Mn^{III} ions and, J_{wb} between the Mn^{II} and Mn^{III} ions, within the [Mn$_4$] cluster (Scheme 2). This experimental data can be well reproduced by a simulation curve deduced from the Heisenberg−Van Vleck model that has been already employed by Christou and Hendrickson et al. (the Hamiltonian used here is $\boldsymbol{H} = -2J_{bb}(\boldsymbol{S}_{Mn2}\boldsymbol{S}_{Mn2'}) - 2J_{wb}(\boldsymbol{S}_{Mn1} + \boldsymbol{S}_{Mn1'})(\boldsymbol{S}_{Mn2} + \boldsymbol{S}_{Mn2'})$).[8] The data below 20 K representing a decrease of χT were omitted in the simulation procedure to avoid influence of zero-field splitting (ZFS) effect or intercomplex antiferromagnetic interactions. With temperature-independent paramagnetism (TIP) fixed to 6×10^{-4} cm^3·mol^{-1}, excellent fits were achieved with final optimized parameters being listed in Table 3 (the red curve in Figure 6). Clearly, all Mn ions of

---

(22) Miyasaka, H.; Clérac, R.; Campos-Fernández, C. S.; Dunbar, K. R. *Inorg. Chem.* **2001**, *40*, 1663.

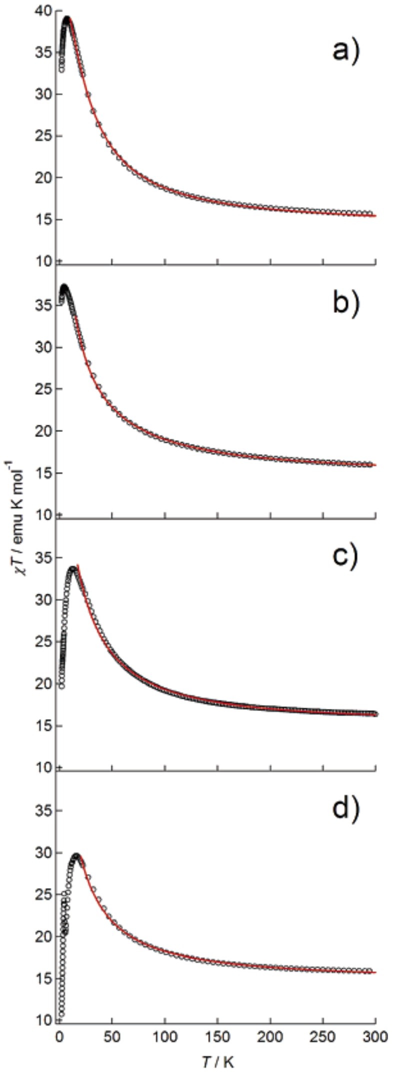

Figure 6. Temperature dependence of χT of **1** (a), **2** (b), **3** (c), and **4** (d) (under 1 kOe). The red solid line represents a simulation curve using the tetranuclear Heisenberg model described in the text.

the $[Mn_4]$ unit in **1**−**4** are ferromagnetically coupled ($J_{bb} > J_{wb} > 0$) to give an $S_T = 9$ ground state. The values of J_{wb}, J_{bb}, and g are similar to those reported in the literatures.[5d,8,9]

Single-Molecule Magnet Behavior in 1 and 2. Alternating current (ac) susceptibility was measured on polycrystalline samples of **1** and **2** under 3 Oe oscillation field and zero dc field as a function of temperature and frequency. Figure 7 shows the temperature dependence of ac susceptibility for **1** and **2**. Both compounds possess frequency-dependent in-phase (χ') and out-of-phase (χ'') susceptibilities, which are a signature of the magnetization slow relaxation, i.e. SMM behavior by analogy to related $[Mn_4]$ compounds.[5,8,9] However in **1** and **2**, the blocking temperature does not reach 1.8 K even at 1500 Hz. Similar behavior has been already observed in $[Mn_4(hmp)_6(H_2O)_2Br_2]Br_2{\cdot}4H_2O$,[8a,b] $[Mn_4(hmp)_4(MeO)_2(acac)_2](ClO_4)_2{\cdot}4MeOH$,[8c] $[Mn_4(hmp)_6(MeCN)_2(NO_3)_2](ClO_4)_2{\cdot}4MeCN$,[8c] or $[Mn_4(hmp)_6(NO_3)_4]{\cdot}MeCN$.[8c] Quite commonly, the characteristic relaxation time of a SMM is easily deduced from the maximum of the χ'' vs T data at a given frequency.[1,2] To get an estimation of the characteristic relaxation time in the absence of such maxima in the χ'' vs T, we used simulation curves obtained by a generalized Debye model for the frequency dependence of the ac susceptibility (χ'' vs ν) measured at different temperatures (Figure S1).[23] As expected for the $[Mn_4]$ SMM, the deduced relaxation time (Figure S2) follows a thermally activated behavior (Arrhenius): $\tau = \tau_0 \exp(\Delta_{eff}/k_BT)$ with $\tau_0 = 5.64 \times 10^{-7}$ s, $\Delta_{eff}/k_B = 12.3$ K and $\tau_0 = 2.23 \times 10^{-7}$ s, $\Delta_{eff}/k_B = 12.8$ K for **1** and **2**, respectively.

Scheme 2. Schematic Spin Topology with the Definition of the Intra-cluster Magnetic Interactions

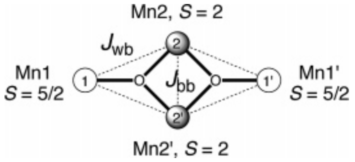

In SMMs, quantum tunneling of the magnetization (QTM) becomes the only pathway of relaxation at very low temperatures. Experimentally, a crossover occurs between the quantum and thermally activated regimes called thermally assisted QTM. In this intermediate range of temperature, the thermal barrier is “short-cut” by the quantum tunneling and should be, therefore, viewed as an effective barrier, Δ_{eff}, being smaller than the theoretical energy barrier $\Delta = |D|S_T^2$ (for integer S_T spins), where D is the axial zero-field splitting parameter and S_T is the spin ground state. In the thermally assisted QTM regime, a small dc field is enough to reduce the influence of the quantum path and thus the relaxation time becomes largely dominated by the temperature. On the basis of this hypothesis, we have applied 1500 Oe (Figure S3) and studied the relaxation time using ac susceptibility technique. As expected for ideal SMMs, the relaxation time of both compounds follows activated behavior with an enhanced energy barrier, $\Delta_{eff}/k_B = 18.9$ K and $\Delta_{eff}/k_B = 21.7$ K for **1** and **2**, respectively.

To get an estimation of the D parameter, we have measured the field dependence of the magnetization on polycrystalline samples of **1**−**4** at 1.82 K up to 7 T. Both **1** and **2** display the

Table 3. Magnetic Parameters Obtained for **1**−**4** Together with Related $[Mn_4]$ Complexes

cmpd	g	J_{wb}/k_B [K]	J_{bb}/k_B [K]	Δ_{eff}/k_B [K]	D/k_B [K]^d	ref
1	1.94	1.61	9.80	12.3	−0.34	this work
2	1.97	1.15	12.66	12.8	−0.41	this work
3	1.98	1.30	10.89	−	−	this work
4	1.98	1.02	9.12	−	−	this work
$[Mn_4(hmp)_6(H_2O)_2Br_2](Br)_2{\cdot}4H_2O$	1.94	1.34	12.65	15.8	−0.45	8a, 8b
$[Mn_4(hmp)_4(MeO)_2(acac)_2](ClO_4)_2{\cdot}4MeOH$	1.93	1.1	7.6	−	−0.31	8c
$[Mn_4(hmp)_6(MeCN)_2(NO_3)_2](ClO_4)_2{\cdot}4MeCN$	1.87	1.4	14.2	−	−0.27	8c
$[Mn_4(hmp)_6(NO_3)_4]{\cdot}MeCN$	1.99	6.0	9.1	−	−0.31	8c
$[Mn_4(hmp)_6(CH_3CN)_2(H_2O)_4](ClO_4)_4{\cdot}2CH_3CN$	1.96	0.66(1)	8.56(5)	23.3	−0.33	9
$[Mn_4(hmp)_6(H_2O)_2(NO_3)_2](NO_3)_2{\cdot}2.5H_2O$	1.96	0.80(5)	7.1(1)	20.9	−0.35	5d

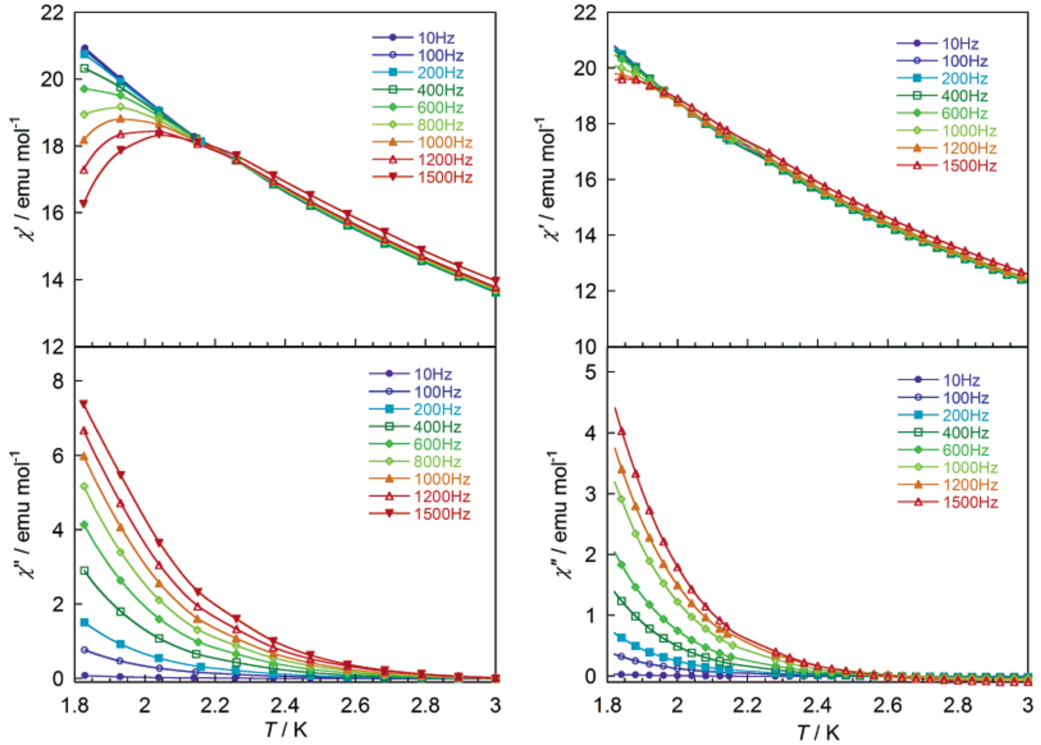

Figure 7. Temperature and frequency dependence of the real (χ') and imaginary (χ'') parts of the ac susceptibility for **1** (left) and **2** (right). The solid lines are guide for the eyes.

same type of behavior (Figure S4): The magnetization increases steeply at initial low fields and then gradually reaches 17.3 μ_B for **1** and 17.5 μ_B for **2** at 7 T. Note that field hysteresis of the magnetization was not observed for both compounds even at 1.82 K. To confirm the nature of the spin ground state and the value of the D parameter, the reduced magnetization at high fields (1−7 T) and low temperatures (1.8−4.5 K) was investigated (Figure 8). The best fit by a matrix-diagonalization method taking into account only the $S_T = 9$ ground state and its axial zero-field splitting term (DS_{Tz}^2) resulted in $g_{av} = 1.97$, $D/k_B = -0.34$ K for **1** and $g_{av} = 2.01$, $D/k_B = -0.41$ K for **2**. The obtained D values are similar to those obtained for the same [Mn_4] SMM family (Table 3) and allow an estimation of the theoretical SMM energy barrier $|D|S_T^2/k_B$ for **1** and **2**, 28 and 34 K, respectively. These values are still significantly higher than those obtained experimentally, indicating that, even under moderated dc fields, the quantum tunneling of the magnetization is still operative.

Although the crystal structures of both compounds are completely different from each other as the discrete [Mn_4] complex for **1** and the covalently bonded 2D network of [Mn_4] complexes for **2**, the dc and ac measurements show that these two compounds possess essentially the same SMM behavior intrinsic to quasi-isolated [Mn_4] units.

Magnetic Ordering in 4. The low-temperature magnetic properties of **4** have been first studied using ac susceptibility measured in zero dc field and with an ac field of 3 Oe. Both χ' and χ'' components exhibit a sharp peak around 4.3 K and at 4.6 K, respectively (Figure 9). The intensity of the ac response is significantly frequency dependent, but the temperature of the peaks remains quasi-constant. This feature contrasts clearly with the SMM behavior observed for **1** and **2** and strongly suggests the presence of a magnetic order at 4.6 K in **4**. To further investigate the properties below 4.6 K of **4**, we have performed a detailed analysis of its M vs H data. At 1.82 K (Figure 10), the initial magnetization increases rapidly at very low fields up to about 0.9 μ_B (at 1 kOe) indicating the presence of the spontaneous magnetization. Then, the magnetization slowly

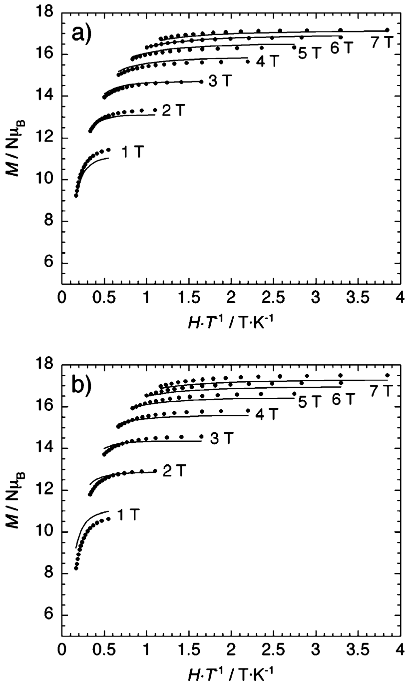

Figure 8. Plots of M vs H/T (between 1.8 and 4.5 K) for **1** (a) and **2** (b). The solid lines are the best fit of the data obtained for $S_T = 9$ with $g = 1.97$, $D/k_B = -0.34$ K for **1** and $g = 2.01$, $D/k_B = -0.41$ K for **2**.

---

(23) (a) Cole, K. S.; Cole, R. H. *J. Chem. Phys.* **1941**, *9*, 341. (b) Boettcher, C. J. F. *Theory of electric polarisation*; Elsevier: Amsterdam, 1952. (c) Aubin, S. M.; Sun, Z.; Pardi, L.; Krzysteck, J.; Folting, K.; Brunel, L.-J.; Rheingold, A. L.; Christou, G.; Hendrickson, D. N. *Inorg. Chem.* **1999**, *38*, 5329.

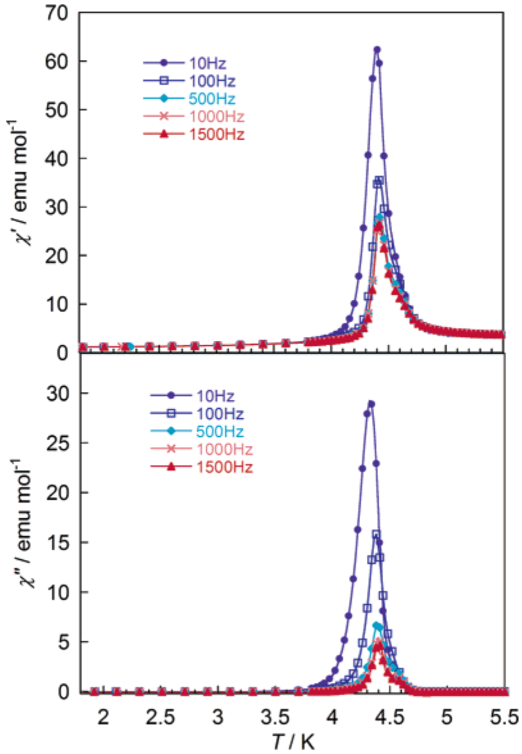

Figure 9. Temperature and frequency dependence of the real (χ') and imaginary (χ'') parts of the ac susceptibility for **4**. The solid lines are guide for the eyes.

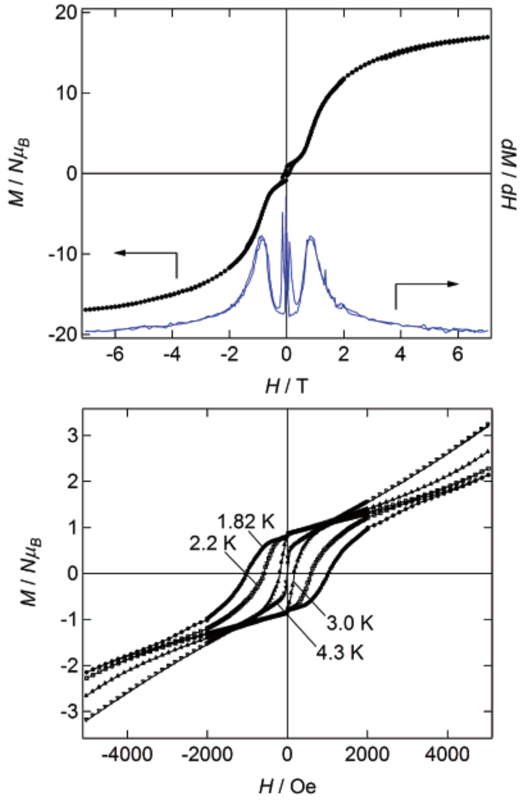

Figure 10. (Top) plots of M vs H and dM/dH vs H for **4** at 1.82 K. (Bottom) Field hysteresis loops of the magnetization for **4** at different temperatures.

reaches an inflection point at 8200 Oe, highlighting antiferromagnetic interactions between the [Mn_4] moments. At higher fields, the magnetization tends to saturate, but only reaches 16.9 μ_B at 7 T. This value is lower than the expected one (17.6 μ_B taking $g = 1.98$ from Table 3) for all aligned $S_T = 9$ [Mn_4] moments, indicating that 7 T is not enough to overcome the anisotropy of the system.

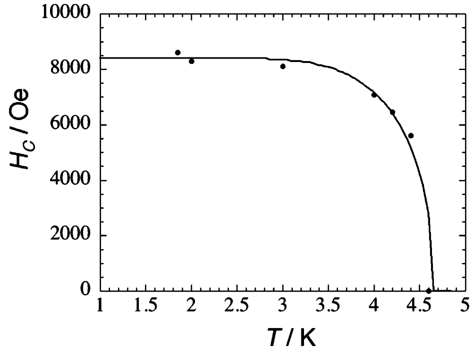

Figure 11. Temperature dependence of the critical field H_C for **4** deduced from the M vs H data at different temperatures. The solid line is a guide for the eyes.

The field hysteresis of the magnetization have been observed below about 4.3 K as shown in Figure 10 (at 1.82 K, coercive field: 1 kOe) with small values of the remnant magnetization (M_R), e.g. 0.87 μ_B at 1.82 K. Considering the shape of the hysteresis loop, M_R is also a good approximation for the spontaneous magnetization. The presence of (i) only one type of magnetic species ([Mn_4] unit with the $S_T = 9$ macro-spin), (ii) antiferromagnetic interactions, and (iii) spontaneous magnetization, explains well a canting of the magnetic moments as already emphasized by the structural description (vide supra) that revealed the two orientations of the Jahn Teller axes (each of which corresponds to a local easy-axis of the [Mn_4] magnetization). With the spontaneous magnetization of 0.87 μ_B at 1.82 K and an expected saturation value of 18 μ_B, the angle between the two spin orientations can be estimated at about 11°,[24] in good agreement with the structural description and the angle of 18° found between the Jahn–Teller axes (this angle will be noted θ in the following). Furthermore, the angle between the two local easy axes was confirmed by angle variations of the magnetization measured on single crystals of **2**, **3**, and **4** (Figure S5).

The inflection point on the M vs H data observed around 8200 Oe (H_C) at 1.82 K is reminiscent of the spin-flip transition in metamagnetic systems. Therefore, the study of H_C with the temperature has been performed and led to a phase diagram typically seen for metamagnetic compounds (Figure 11).[25] As already suggested by the ac susceptibility and the low field M vs H data (vide supra), a Paramagnetic (P)–Canted Antiferromagnetic (CAF) phase transition is observed at 4.6 K in the absence of dc field. When the magnetic field is applied, a transition line, $H_C(T)$, is found corresponding to the saturation of the magnetization, i.e., to the CAF–P phase transition. This instability occurs when the applied field overcomes the effect of the antiferromagnetic coupling (J) between the [Mn_4]

---

(24) In the limit of vanishing dc field, the spontaneous magnetization for a powder sample (M_S) is $M_Z/2$ where M_Z is the magnitude of spontaneous magnetization for a single crystal. For a given splitting angle (θ) between the two spin orientations, M_Z is related to the magnetization at saturation (M_{sat}) by $M_Z = M_{sat}\sin(\theta/2)$ at $T = 0$ K; therefore $\theta = 2\,\mathrm{invsin}(2\,M_S/M_{sat})$.

(25) Stryjewski, E.; Giordano, N. *Adv. Phys.* **1977**, *26*, 487.

complexes and can thus be expressed in the Ising limit at 0 K as:[26]

$$H_C(0) = \frac{2|zJ|S_T}{g\mu_B}\frac{\cos(\theta)}{\cos(\theta/2)} \qquad (1)$$

where z is the number of neighboring spins and S_T is the spin ground state of the magnetic unit. Taking $H_C(1.82\ \mathrm{K}) = 8200$ Oe as a good approximation of its value at 0 K and $\theta = 11°$, the magnetic interaction between the anisotropic [Mn$_4$] units is $zJ/k_B \approx -0.06$ K. Based on the crystal structure of **4**, these magnetic interactions are more likely to be mediated by the dicyanamide links in the 2D arrangement than through space and weak interlayer π-π contacts. Indeed, this exchange through the dicyanamide linkage like [Mn^{II}−NC−N−CN−Mn^{II}] is well-known to be weakly antiferromagnetic (∼−0.1 K),[27] in good agreement with the obtained value. The theoretical critical temperature in zero field for a 2D square lattice Ising model[28] is known and can be calculated from:

$$T_C = 0.56730 \times T_{CM} \qquad (2)$$

where $T_{CM} = 2|zJ|S_T^2 \cos(\theta)/k_B$ is the critical temperature of the Ising model obtained in the frame of the mean field approximation. Using the zJ (−0.06 K) deduced from the critical field H_C(1.82 K), the theoretical value of T_C is thus 5.4 K. This estimation is in relatively good agreement with the experimental T_C (4.6 K) considering that a small overestimation is expected using the Ising model, while our experimental system assumes as a finite anisotropic system. In summary, the combined ac and dc measurements on **4** show unambiguously the presence of a magnetic long-range order below 4.6 K corresponding to the canted antiferromagnetic ground state.

Interplay between SMM Behavior and Magnetic Order in 3. As shown in a *MH* curve of Figure 12, the magnetization of **3** at 1.82 K increases rapidly at low fields (∼100 Oe) and then further to reach 15.3 μ_B at 7 T. Below 2.1 K, small field hysteresis loops of the magnetization are present (at 1.82 K, coercive field: 20 Oe). At 3800 Oe, a “weak” inflection point (emphasized by the maximum obtained on the d*M*/d*H* vs *H* plot) is observed on the magnetization at 1.82 K (Figure 12). Increasing the temperature, this feature becomes steeply and impossible to detect above 1.9 K. This behavior is similar to that observed for **4**, and we have, therefore, used eq 1 to determinate the coupling (zJ) between the adjacent [Mn$_4$] units bridged by the dcn$^-$ ligands. Considering the canting angle quoted in the structural section ($\theta = 63°$), the obtained zJ is about −0.05 K. It should be emphasized that this value is very close to the one obtained for **4** or for related compounds possessing the [Mn^{II}−NC−N−CN−Mn^{II}] bridge.[27] Considering $zJ/k_B \approx -0.05$ K, eq 2 estimates a theoretical transition temperature of this 2D compound of 2.1 K, in perfect match with the vanishing of the hysteresis loops (Figure 12). Hence, by analogy with the magnetic behavior of **4**, the static properties of **3** suggest the presence of a canted antiferromagnetic order below 2.1 K.

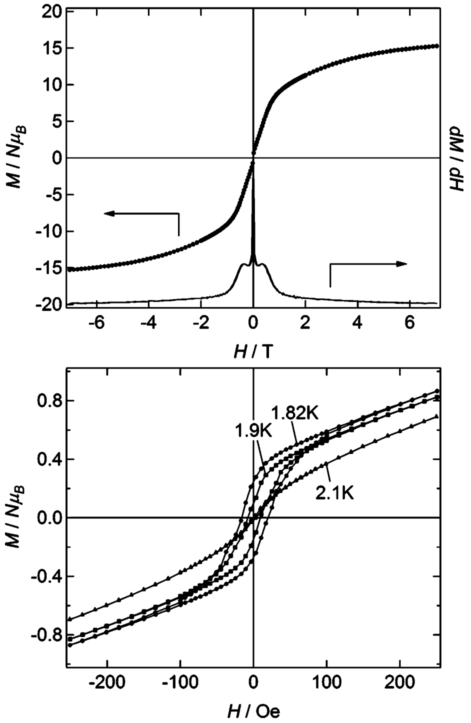

Figure 12. (Top) Plots of *M* vs *H* and *dM*/d*H* vs *H* for **3** at 1.82 K. (Bottom) Field hysteresis loops of the magnetization for **3** at different temperatures.

To get more insight into the magnetic properties of **3**, ac susceptibility measurements have also been performed (Figure 13, left) and shown a strong frequency dependence of both χ' and χ'' components indicating slow relaxation of the magnetization. It is interesting to note that a crossover is observed when the maximum of $\chi''(T)$ reaches $T_{max} = 2.1$ K for 30 Hz. At higher and lower frequencies, the T_{max} is increasing and decreasing, respectively, but with a declining intensity in both cases. As usually done for SMMs, we have attempted to obtain a characteristic relaxation time from the maximum of the χ'' vs T data at a given frequency. For this compound, the resulting time does not follow the Arrhenius dependence. To understand this feature, the frequency dependences of the ac susceptibility (χ'' vs ν) have been performed at a given temperature (Figure 13, right).

Between 1.85 and 2.3 K, the χ'' vs ν data revealed the presence of two modes of relaxation in the 0.01−1500 Hz

---

(26) This expression can be obtained easily from the simple Ising antiferromagnetic case where the critical field is $g\mu_B H_C(0) S_T = 2zJS_T^2$ (Chikazumi, S. *Physics of Ferromagnetism*; Clarendon Press: Oxford Science Publications: Oxford, 1997; p 521). Due to the canting between the two [Mn$_4$] orientations, the projection of the magnetic field on the two resulting magnetic moments becomes the effective applied field seen by each sublattice. Therefore $H_C(0)$ should be replaced in the previous equation by $H_C(0)\cos(\theta/2)$. The exchange interaction between the two nonparallel [Mn$_4$] moments is also renormalized by the canting angle to lead to an effective magnetic interaction $J\cos(\theta)$. Equation 1 is simply obtained by replacing these two renormalized components in the above equation.

(27) (a) Schlueter, J. A.; Manson, J. L.; Hyzer, K. A.; Geiser, U. *Inorg. Chem.* **2004**, *43*, 4100. (b) Manson, J. L.; Incarvito, C. D.; Rheingold, A. L.; Miller, J. S. *J. Chem. Soc., Dalton Trans.* **1998**, 3705. (c) Batten, S. R.; Jensen, P.; Kepert, C. J.; Kurmoo, M.; Moubaraki, B.; Murray, K. S.; Price, D. J. *J. Chem. Soc., Dalton Trans.* **1999**, 2987. (d) Claramunt, A.; Escuer, A.; Mautner, F. A.; Sanz, N.; Vicente, R. *J. Chem. Soc., Dalton Trans.* **2000**, 2627. (e) Sun, B.-W.; Gao, S.; Ma, B.-Q.; Niu, D.-Z.; Wang, Z.-M. *J. Chem. Soc., Dalton Trans.* **2000**, 4187. (f) Raebiger, J. W.; Manson, J. L.; Sommer, R. D.; Geiser, U.; Rheingold, A. L.; Miller, J. S. *Inorg. Chem.* **2001**, *40*, 2578. (g) Escuer, A.; Mautner, F. A.; Sanz, N.; Vicente, R. *Inorg. Chem.* **2000**, *39*, 1668. (h) Marshall, S. R.; Incarvito, C. D.; Manson, J. L.; Rheingold, A. L.; Miller, J. S. *Inorg. Chem.* **2000**, *39*, 1969. (i) van der Werff, P. M.; Batten, S. R.; Jensen, P.; Moubaraki, B.; Murray, K. S. *Inorg. Chem.* **2001**, *40*, 1718. (j) Lin, H.-H.; Mohanta, S.; Lee, C.-J.; Wei, H.-H. *Inorg. Chem.* **2003**, *42*, 1584. (k) Manson, J. L.; Arif, A. M.; Incarvito, C. D.; Liable-Sands, L. M.; Rheingold, A. L.; Miller, J. S. *J. Solid State Chem.* **1999**, *145*, 369. (l) Dalai, S.; Mukherjee, P. S.; Zangrando, E.; Chaudhuri, N. R. *New J. Chem.* **2002**, *26*, 1185.

(28) Domb, C. In *Phase transition and critical phenomena*; Domb, C., Green, M. S., Eds.; Academic Press: London, New York, 1974; Vol. 3, Chapter 6, p 357.

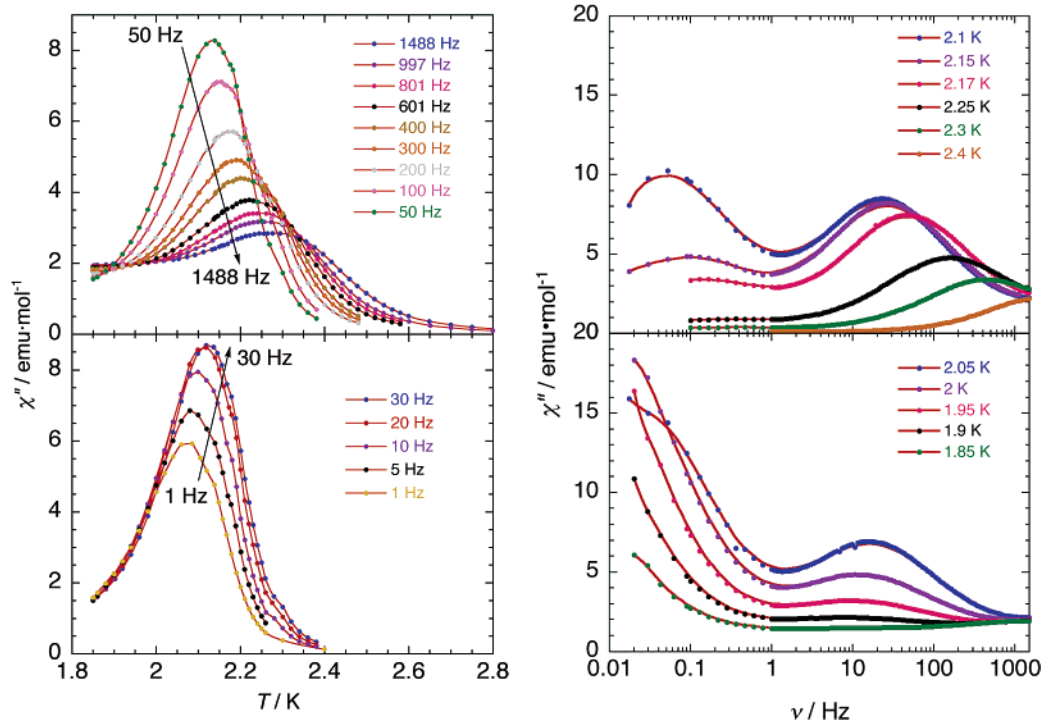

Figure 13. Temperature (left) and frequency (right) dependence of the imaginary (χ'') parts of the ac susceptibility for **3**. The solid lines are guide for the eyes.

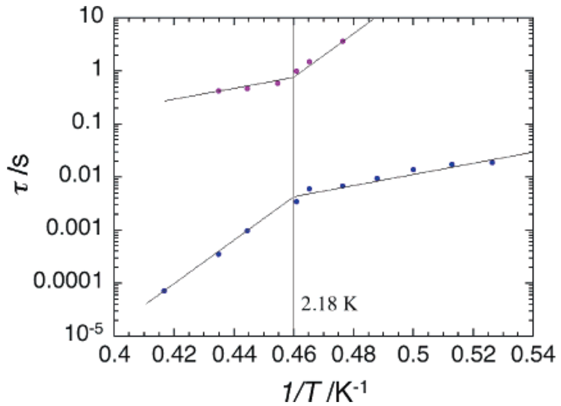

Figure 14. τ vs *1/T* plot for **3** deduced from the low frequency (purple ●) and high frequency (blue ●) modes observed on the χ'' vs ν data.

frequency window that prevent a simple analysis of the relaxation time using $\chi''(T)$ data. But, using the maximum of $\chi''(\nu)$ at a given temperature (Figure 13), the two relaxation processes can be obtained as shown in Figure 14 (purple and blue dots). Both relaxation processes exhibit a clear crossover around 2.2 K. The low and high-frequency modes (corresponding to purple and blue dots, respectively, in Figure 14) follow activated behaviors, above 2.2 K, with $\tau_0 = 2.2 \times 10^{-4}$ s, $\Delta/k_B = 17$ K and $\tau_0 = 6 \times 10^{-21}$ s, $\Delta/k_B = 89$ K, respectively, and below 2.2 K, with $\tau_0 = 2.4 \times 10^{-17}$ s, $\Delta/k_B = 83$ K and $\tau_0 = 3.4 \times 10^{-7}$ s, $\Delta/k_B = 21$ K, respectively. The origin of these two relaxation modes is not yet well understood even if such a feature has been already observed and analyzed in $[Mn_4Cl_4(L')_4]$ (H_2L' = 4-*tert*-butyl-salicylidene-2-ethanolamine) by Boskovic et al.[29] In this compound, the crossover has been obtained on the ac data at the critical temperature of the ferromagnetic ground state. A strong analogy between this behavior and the one of **3** as static properties suggests the presence of an antiferromagnetic order below 2.1 K (see Figure 6), a temperature at which the ac data experience a clear crossover.

To further investigate the presence of the magnetic order in **3** with concomitant slow relaxation of the magnetization, heat capacity measurements have been performed and compared among the 2D [Mn₄]-based compounds (**2**−**4**).

Single-Crystal Heat-Capacity Calorimetry of 2−4. Heat-capacity measurements for **2**−**4** were carried out on a single crystal in the temperature range of 0.4−12 K by a thermal relaxation method in a ^{3}He cryostat. Figure 15a shows the temperature dependence of C_p for **2**−**4** measured at zero-applied field. For **2** and above 1.8 K, a broad hump is observed around 2.5 K as already seen for SMM complexes.[30−33] Such a broad feature is usually attributed to the Schottky heat capacity originated from the energy scheme of the [Mn₄] unit spin levels. Since the value of D/k_B in **2** is −0.41 K, the energy separation (δ) between the ground state ($m_s = \pm 9$) and the first excited state ($m_s = \pm 8$) is 6.97 K. The two-levels Schottky heat capacity is known to form a broad peak at about 0.4δ, in good agreement with the experience (2.5 K).[34] Besides this contribution, the observed heat capacity should also contain magnetic and lattice components. However, below 0.9 K, a slight increase of C_p is

---

(29) Boskovic, C.; Bircher, R.; Tregenna-Piggott, P. L. W.; Güdel, H.; Paulsen, C.; Wernsdorfer, W.; Barra, A. L.; Khatsko, E.; Neels, A.; Stoeckli-Evans, H. *J. Am. Chem. Soc.* **2003**, *125*, 14046.

(30) Miyazaki, Y.; Bhattacharjee, A.; Nakano, M.; Saito, K.; Aubin, S. M. J.; Eppley, H. J.; Christou, G.; Hendrickson, D. N.; Sorai, M. *Inorg. Chem.* **2001**, *40*, 6632.

(31) Bhattacharjee, A.; Miyazaki, Y.; Nakano, M.; Yoo, J.; Christou, G.; Hendrickson, D. N.; Sorai, M. *Polyhedron* **2001**, *20*, 1607.

(32) Gomes, A. M.; Novak, M. A.; Sessoli, R.; Caneschi, A.; Gatteschi, D. *Phys. Rev. B* **1998**, *57*, 5021.

(33) Fominaya, F.; Villain, J.; Fournier, T.; Gandit, P.; Chaussy, J.; Fort, A.; Caneschi, A. *Phys. Rev. B* **1999**, *59*, 519.

(34) Gopal, E. S. R. *Specific Heats at Low Temperatures*; Plenum Press: New York, 1966; pp 102−105.

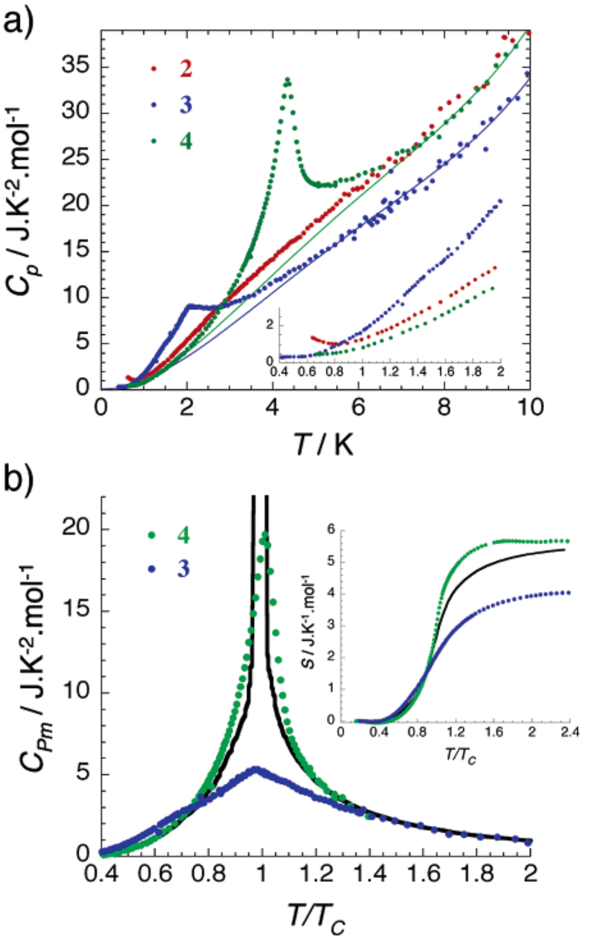

Figure 15. (a) C_p vs T data for **2** (red ●), **3** (blue ●), and **4** (green ●) measured on a single crystal under zero-applied field. The green and blue solid lines are the empirical baselines that have been used to determine the critical part of the heat capacity (C_{Pm}) and the resulting magnetic entropy (S). (Inset) Zoom of the C_p vs T plots between 0.4 and 2 K. (b) C_{Pm} vs T/T_C data for **3** (blue ●) and **4** (green ●) (T_C has been taken equal to 2.0 and 4.3 K, respectively). (Inset) Magnetic entropy (S) vs T/T_C plots. The black solid line is the C_p and S expected for a 2D square Ising model.[36]

observed reproducibly. Such behavior is expected to be a possible transition from the precursor to a short-range or a long-range magnetic order below 0.6 K. This is indeed not a surprise because the 2D network of **2** is similar to those of **3** and **4**. Considering that the canted angle between the two Jahn−Teller axes is about 80° for **2** (see structural part) and that the exchange through the dicyanamide linkage in [$Mn^{II}-NC-N-CN-Mn^{II}$] should not be considerably different from the ones obtained for **3** and **4** ($zJ/k_B \approx -0.05(1)$ K), the use of eq 2 leads to a theoretical ordering temperature of about 0.8 K for **2**. It is worth noting that Yamaguchi et al. have observed similar behavior in the [$Mn_4(hmp)_6Br_2(H_2O)_2]Br_2\cdot 4H_2O$ SMM by the heat-capacity calorimetry and magnetic measurements, i.e. showing the presence of its SMM behavior below 2 K followed by an antiferromagnetic transition at 1.33 K.[35]

As shown in Figure 15b, the heat capacity measured for **3** and **4** exhibits a peak located respectively around 2.0 and 4.3 K in zero-applied field, while both disappear under 8 T. To analyze this phenomenon suggesting the presence of a magnetic order, the critical part of the heat capacity (noted in the following: C_{Pm}) must be separated from the regular background. Indeed, two contributions, at least, are present in this regular part: the Schottky component discussed above for **2** ($C_{schottky}$) and the lattice contribution ($C_{lattice}$). Due to the difficulty to estimate accurately these two contributions, we have decided rather to apply an empirical correction using a fourth order polynomial expression (see solid lines in Figure 15a) to obtain C_{Pm} shown in Figure 15b. Comparing the experimental C_{Pm} and the critical specific heat expected for the 2D square lattice Ising model[36] in Figure 15b, these peaks appears to be of similar width with their "wings" in good agreement with the theory. The integration of C_{Pm}/T with respect to temperature gives the temperature dependence of the magnetic entropy, S, as shown in the inset of Figure 15b for **3** and **4**. The saturation value of S for **3** is found to be 4.0 J·K^{-1}·mol^{-1} and 5.7 J·K^{-1}·mol^{-1} at $T/T_C = 2.4$. The latter value is comparable with the maximum entropy of free $m_s = \pm 9$ Ising spins, $R \ln 2 = 5.76$ J·K^{-1}·mol^{-1}. Hence, in agreement with the magnetic properties of **4** described above, the shape (typical λ-type) of heat capacity peak and its associated magnetic entropy confirm the occurrence of a long-range order at 4.3 K. For **3**, the conclusion is not so straightforward. The reproducible observation of the heat capacity peak on several samples of **3** suggests the presence of a magnetic transition around 2 K, but only a rounded maximum is obtained in the critical region (Figure 15b). This result may be indicative of finite size effects or disorder that limits the growth of the correlation length and, therefore, prevents the stabilization of a long-range order. However, this hypothesis might not be realistic. For example, the work of Tanaka et al. (see Figure 9 of ref 36b) on the finite size model shows that an extremely small network should be considered to explain the present experimental data. In any case, the slow dynamics (the SMM behavior) of the isolated [Mn_4] complexes strongly suggests another possibility. As discussed by Zurek,[37] the relaxation time and the correlation length can saturate when approaching a critical point, as an experiment is always made at a finite time scale. Therefore, at the time scale of the heat capacity measurement, which is in the order of 10^2 s in the present experiments, the system might not be at the thermodynamic equilibrium close to the critical point. The correlation length can thus be frozen out and the divergence of the specific heat smoothed out. In other words, the slow relaxation of the magnetization observed in **3** by the ac susceptibility measurements is probably the signature of the dynamics generated by the [Mn_4] moment that is slowly trying to order. Approaching the critical point, this dynamics becomes too slow to follow the continuous line shown in Figure 15b.[38]

Concluding Remarks

We report in this paper the first examples of covalently linked 2D networks of SMMs using double-cuboidal [Mn_4] SMMs and the dcn$^-$ ligand. The chemistry of this system was studied in

---

(35) Yamaguchi, A.; Kusumi, N.; Ishimoto, H.; Mitamura, H.; Goto, T.; Mori, N.; Nakano, M.; Awaga, K.; Yoo, J.; Hendrickson, D. N.; Christou, G. *J. Phys. Soc. Jpn.* **2002**, *71*, 414.

(36) (a) Onsager, L. *Phys. Rev.* **1944**, *65*, 117. (b) Tanaka, Y.; Uryu, N. *J. Phys. Soc. Jpn* **1993**, *62*, 1305.

(37) Zurek, W. H. *Nature* **1985**, *317*, 505; Zurek, W. H. *Nature* **1996**, *382*, 296.

(38) The noncritical shape of the thermal anomaly is reproducible when we have measured for different crystals with different sample masses. This fact means the difference of temperature relaxation time does not affect the present result. The behavior around the critical temperature of **3** is not considered as a technical origin but as an intrinsic effect related to the time scale of the thermodynamic experiments.

detail in order to adjust the synthetic conditions to control the coordination number of the dcn$^-$ ligand on the Mn^{II} ion sites. This methodic work was the key to obtain the discrete cluster, $[Mn_4(hmp)_6(NO_3)_2(dcn)_2]\cdot 2MeCN$, **1**; 2D networks $[Mn_4(hmp)_4(Hpdm)_2(dcn)_2](ClO_4)_2\cdot 2H_2O\cdot 2MeCN$, **2**; $[Mn_4(hmp)_4Br_2(OMe)_2(dcn)_2]\cdot 0.5H_2O\cdot 2THF$, **3**; $[Mn_4(hmp)_6(dcn)_2](ClO_4)_2$, **4**; but also the previously reported 3D architecture, $[Mn_4(hmp)_4(\mu_3\text{-}OH)_2][Mn^{II}(dcn)_6]\cdot 2MeCN\cdot THF$.[10] Whereas **1** possesses, as expected, all the characteristic of a SMM below 2.5 K (for frequency lower than 1500 Hz), the three 2D compounds (**2**, **3**, and **4**) exhibit different magnetic and thermodynamic properties. Compounds **2**, **3**, and **4** possess a similar 2D network based on two different orientations of the $[Mn_4]$ units separated by an angle θ ranging from 80 to 18° between the Jahn–Teller axes. On the basis of this angle and similar magnetic interactions between the $[Mn_4]$ complexes through the dcn$^-$ ligand ($zJ/k_B \approx -0.05(1)$ K), we were able to rationalize different magnetic behavior and the critical temperature of these three compounds that possess a canted antiferromagnetic ground state ($T_C < 0.6$ K for **2**, ≈ 2.1 K for **3**, and ≈ 4.6 K for **4**). For the small θ angle such as 18° (compound **4**), the magnetic interactions are efficient, and the magnetic order occurs easily in a temperature region where the dynamics of the $[Mn_4]$ units is fast. The picture is quite different for **2** and **3** that possess larger canting angles and thus lower *effective* magnetic interactions. In these cases, their magnetic order, which is expected to be stabilized at lower critical temperature, becomes difficult to achieve during the characteristic experimental time due to the intrinsic slow dynamics of the $[Mn_4]$ complexes. As far as we know, these series of compound bring the first experimental evidence of the intimate interplay between a magnetic order and slow relaxation of the magnetization induced by SMM units. As previously mentioned,[10] the use of SMMs as building blocks to design magnetic materials leads to new magnetic behaviors involving a competition between dynamics properties and the thermodynamic equilibrium.

Acknowledgment. We thank Prof. Takayoshi Kuroda-Sowa (Kinki University, Osaka, Japan) for simulations of the reduced magnetization. This work was supported by the PRESTO (H.M.) and CREST projects (H.M., Y.N., and M.Y.) of the Japan Science and Technology Agency (JST) and a Grant-in-Aid for Scientific Research on Priority Areas (No. 17036054 "Chemistry of Coordination Space") from the Ministry of Education, Culture, Sports, Science, and Technology, Japan (H.M.). R.C., L.L., and C.C. thank the CNRS, the University of Bordeaux 1 and the Conseil Regional d'Aquitaine for financial support and Dr. Olivier Roubeau for stimulating discussions.

Supporting Information Available: Cyrstallographic data for **1**–**4** (CCDC-287894 for **1**, -287895 for **2**, -287896 for **3**, and -287897 for **4**) are also available free of charge via www.ccds.cam.ac.uk/conts/retrieving.html (or from the Cambridge Crystallographic Data Center, 12, Union Road, Cambridge CB21EZ, UK; fax:(+44) 1223-336-033, or deposit@ccdc.cam.ac.uk). X-ray crystallographic files (CIF) for **1**–**4**; magnetic data (Figures S1–S5). This material is available free of charge via the Internet at http://pubs.acs.org.

JA0574062